JJMIE

Volume 19, Number 1, March. 2025
ISSN 1995-6665
Pages 41 – 65
https://doi.org/10.59038/jjmie/190104
Editor-in-Chief: Prof. Ali M. Jawarneh

Jordan Journal of Mechanical and Industrial Engineering

Techno-economic Evaluation of an Innovative Integrated System for Water and Power Supply in Sudan under Variable Climatic Conditions

Moataz Abdelgadir Ali[a], Iman El Gheriany[b], Wael M. El-Maghlany[a], Mohammed El-Adawy[c,*]

[a] Mechanical Engineering Department, Faculty of Engineering, Alexandria University, Egypt.
[b] Chemical Engineering Department, Faculty of Engineering, Alexandria University, Egypt.
[c] Interdisciplinary Research Center for Hydrogen Technologies and Carbon Management (IRC-HTCM), King Fahd University of Petroleum & Minerals, Dhahran, Saudi Arabia

Received 28 Jul 2024 *Accepted 11 Dec 2024*

Abstract

This research investigates the potential of integrating a combined cycle power plant with a hybrid MSF-RO desalination system in Port Sudan. The proposed system utilizes waste heat from the power plant's heat recovery steam generator to drive the MSF desalination process. By leveraging waste heat from the power plant's flue gas, the aim is to enhance sustainability and address water scarcity. A detailed simulation of the plant is performed using Aspen HYSYS 10, assessing the monthly variations in power and water production due to changes in ambient air temperature, seawater temperature, and salinity in Port Sudan. The MSF unit contributes at least 7,574 m³/day of freshwater in September to the 12,600 m³/day produced by the RO unit. The highest freshwater productivity of the MSF unit occurs in February, reaching 8,025 m³/day. Maximum freshwater generation coincides with peak net power production and combined cycle efficiency. In September, adverse weather conditions negatively impact both the combined power cycle and the evaporation range of the MSF unit, resulting in minimal freshwater production. The highest fuel costs, amounting to $256,818 per month, and the penalty costs for NOx emissions, reaching $101,655 per month, occur in January, February, and December. The shortest payback period is 4.075 years, occurring in February. Revenue is lowest in July when net power production is at its minimum.

.

Keywords: Waste heat recovery; Combined cycle power plant; MSF plant; Hybrid MSF-RO desalination; MSF-OT simulation; Techno-economic analysis; Aspen HYSYS simulation.

Nomenclature

A	Heat transfer area	m^2
C	Cost	\$
$\dot{C}$	Annual cost	\$/year
c_{el}	Price of electricity	$\$.(kWh)^{-1}$
c_{fuel}	Price of natural gas	$\$.(GJ)^{-1}$
c_{NO_X}	Penalty cost factor	$\$.(kgNO_X)^{-1}$
c_w	Price of water	$\$.(m^3)^{-1}$
D_n	vapor flow rate	$kg.(h)^{-1}$
GH	Gate height	m
H	Height of the brine pool	m
i	Interest rate	%
$\dot{m}$	Mass flow rate	$kg.(h)^{-1}$
n	Number of effects	
$P.P$	Pump power	kW
q	Plant life	year
Q	Heat transfer	Kw
SW	Stage width	m
$\dot{S}$	Annual income	\$/year
T	Temperature	℃ or K
V_b	Brine flow rate per unit length of the chamber width	$kg.(m.s)^{-1}$
V_{V_n}	Vapor allowable velocity	$m.(s)^{-1}$
W	Power	kW
X	Salt concentration	PPM
Y	Time of operation	day/year

Subscripts

ac	annual investment cost
av	Average
b	Brine
cw	Cooling water
cm	Contingency
co	Construction overhead
d	Distillate
di	Direct
de	Desalination
dim	Demister
EC	Economizer
EV	Evaporator

* Corresponding author e-mail: mohammed.eladawy@kfupm.edu.sa.

el	Electrical
eq	Equipment
f	Feed
fr	Freight
g	Gas
id	Indirect
In	Investment
la	Land
$loss$	Thermodynamic loss (loss)
NG	Natural gas
ow	Owner
pp	Payback period
s	Steam
sd	Site construction
SH	Super heater
sw	Seawater
v	Vapour
w	Water

Greek symbols

β	Coefficient of M&O cost
ξ	Inflation factor
ρ	Density
η	Efficiency
η_s	Isentropic efficiency
r_p	Pressure ratio
ΔT	Temperature difference
C_d	Friction coefficient
C_b	Heat capacity of liquid streams
π	Osmotic pressure
k_s	Salt permeability
k_w	Membrane water permeability

Abbreviations

AC	Air compressor
ADS	Adsorption desalination system
BPE	Boiling point elevation
CC	Combustion chamber
CON	Condenser
CRF	Capital recovery factor
FF	Membrane fouling factor
FFC	Fuel Flow Control
GT	Gas turbine
$GTCC$	Gas turbine combined cycle
$G.T.E$	Gas Turbine Engine
$HRSG$	Heat recovery steam generator
L	Length
LHV	Lower heating value
MD	Membrane distillation
MED	Multi-effect desalination
$MENA$	Middle East and North Africa
MSF	Multi-stage flash
NEA	Non equilibrium allowance
$MSF-OT$	Once-through MSF unit
P	Pressure
PR	Performance ratio
$PRSV$	Peng-Robinson-Stryjek-Vera's
PV/T	photovoltaic thermal
RO	Reverse osmosis
$SADS$	Solar adsorption desalination system
$SDSE$	Solar dish Stirling engine
$SDSPSEDS$	Solar dish/Stirling-powered single-effect distillation system
SM	Supplementary Material
ST	Steam turbine
$S.T.E$	Steam Turbine Engine
TAC	Total annual cost
TFC	Temperature correction factor
TIT	Turbine Inlet Temperature
TVC	Thermal vapour compression
UF	Utilization factors

1. Introduction

Achieving the 2030 sustainable development goals of clean water and affordable clean energy in the Middle East and North Africa necessitates effective management of the intricate relationship between water and energy resources[1-3].Rising temperatures, increased water scarcity, and reductions in fossil-fuel consumption subsidies in a region heavily reliant on fossil fuels heighten this challenge[4-7].Coupling power generation with thermal desalination technologies offers a way to reduce the energy required for freshwater production. Power and water cogeneration began by pairing desalination units, such as multi-stage flash (MSF) or multiple-effect desalination (MED), with steam turbine (ST) power plants[8]. When gas turbine combined cycle (GTCC) power plants were adopted in the 2000′s, thermal units were powered by the latent heat of the steam turbine exhaust or by steam extracted from heat recovery steam generator (HRSG). Membrane-based desalination technologies consume nearly four times less energy than thermal processes and dominate the seawater desalination market in the MENA region [9].However, the economic benefit of reverse osmosis (RO) systems heavily depends on raw seawater quality. The high average salinity of the Red Sea and Gulf regions [9, 10]shortens the lifespan of RO membrane modules and requires higher pump pressure for the RO process [9]. Therefore, hybrid desalination units are becoming increasingly important for the future of drinking water and power production in the Middle East[11, 12]. Harnessing solar energy for heating, cooling, and thermal desalination is among the most promising applications of renewable energy technology [4, 13-19]. The hybrid MD-RO system powered by solar energy is a promising integration scheme for sustainable water desalination[20]. Hybrid MSF-RO desalination systems combine the high reliability and capacity of thermal desalination processes with the low energy requirement of membrane processes. Furthermore, these systems contribute to a reduction in desalination's carbon footprint by up to 40% through extended RO membrane lifespan. This eliminates the recurring costs of membrane replacement often associated with high-salinity feedwater [11].

Thermodynamic models of power-water cogenerating systems have largely contributed to the investigation of different dual-purpose plant configurations[8, 21-25]. They provided a base for parametric analysis and multi-objective optimization studies. The case studies differed in the considered process structures, optimization methodologies, and thermodynamic and/or economic optimization criteria[26, 27]. In addition, models were used to optimize the allocation of fuel between water and power production[21, 28-31].

Trigeneration renewable systems provide sustainable solutions for freshwater scarcity, energy shortages, and climate change by producing heat, electricity, and distilled water with minimal environmental impact [32, 33]. A solar dish/Stirling-powered distillation system (SDSPSEDS) demonstrated efficient tri-generation by integrating electricity, heat, and freshwater production [32]. A hybrid system combining reverse osmosis, adsorption desalination, and a solar dish Stirling engine (RO-

ADS/SDSE) enhanced energy efficiency by utilizing waste heat for additional desalination [33]. Additionally, a solar adsorption desalination system (SADS) powered by hybrid PV/T collectors improved both electrical efficiency and desalination performance through optimized thermal integration [34].

The influence of gas turbine partial load operation and varying ambient temperatures on the net power output and freshwater production of combined cycle power plants integrated with thermal desalination units has been the subject of considerable research interest. A recent techno-economic study[35]showed that it is possible to increase the freshwater production capacity of a GTCC-MED-TVC using an RO unit operated by the available electricity not supplied to the grid. The study demonstrated how the RO unit's water production varied with average electricity availability across different time periods and seasons. The focal point in most studies was the effect of variations of ambient air temperature on the power generation cycle[8, 36-39]. A study addressing the effect of weather conditions on the power-water production plant in a holistic manner does not exist.

The main rationale behind the power and water co-generation scheme was initially to improve the efficiency of existing fossil fuel-based energy systems[12, 40]by running the thermal desalination plants using the waste heat from the power cycle. However, in most of the published research, thermal desalination plants integrated to a GTCC power plant used high-energy streams that can contribute to power generation. The desalination unit was practically the condenser of the power cycle[8, 21, 35-37]. To supply the thermal desalination unit with the required process heat input at sufficiently high temperatures that rangefrom 60 and 90 °C for MED units and 90 - 120 °C for MSF units, the condenser of the power cycle was run at significantly higher temperatures. Consequently, the cycle had a relatively reduced electricity output and cycle efficiency[41].This conventional co-generation scheme is not suitable for African countries struggling with energy poverty and frequent power outage. Therefore, it is crucial for countries -like Sudan- to reduce the amount of power allocated for water production in dual-purpose plants[12]. One alternative is to rely on solar energy to power small and medium small-scale thermal desalination plants[42-45]. Based on a case study performed in the UAE, solar energy provided the energy requirement of a small-scale MSF unit producing 1880m^3/day.

Another relevant alternative is the exploitation of the energy of waste streams. The recovery of the energy of waste gases emerging from a refinery plant[46]was evaluated from the thermodynamic and economic standpoint.Tian, et al. [47] recently showed that itwas possible to recover the waste heat of 50,000 kg/hof a GTCC plant exhaust gases at 150°C in the production of 892.4 MWh of electricity and 6,656.8$m^3/year$. The proposed power and water cogeneration scheme involved an Organic Rankine Cycle and an MSF unit[47].

This study addresses two key gaps identified in the literature related to power-water cogeneration. Firstly, there is a lack of focus on optimizing thermal desalination processes powered by the energy of waste gases. Most studies [8, 21, 35-37]rely on high-temperature waste heat to power the thermal desalination units resulting in reduced power output and cycle efficiency. Research is needed to explore the feasibility and efficiency of running these units at lower temperatures using lower-grade waste heat or integrating other heat sources. Secondly, there is a lack of thorough analysis of the combined effect of air and seawater temperatures and salinity levels on the performance of combined power and desalination systems. Understanding these climatic impacts is crucial for optimizing system performance and efficiency. Comprehensive studies focusing on the synergistic effects of climate related variables will offer insights into real-world scenarios and contribute to the design and operation of more resilient cogeneration systems capable of maintaining stable performance despite fluctuating weather conditions.

1.1. Main Contributions and Novelties

The drive for highly fuel-efficient systems is propelled by stringent environmental regulations and escalating fuel costs. Industrial processes often result in significant energy wastage through unburned fuel, heat discharge from drainage water, and notably, heat loss from flue gases. By harnessing and converting this wasted heat into usable energy, industries can significantly reduce emissions and promote sustainable practices. Furthermore, the rising demand for freshwater has led to the development of more energy-efficient desalination technologies. Integrating desalination systems with power plants, particularly combined cycle power plants, has emerged as a promising solution. This study introduces a novel approach to integrating power generation and water desalination by combining a hybrid MSF-RO desalination system with an existing gas turbine combined cycle power plant in Port Sudan. The proposed system innovatively utilizes waste heat from the power plant's heat recovery steam generator to drive the MSF desalination process, fostering a synergistic relationship between electricity production and freshwater generation.

1.2. Key contributions and novelties of this research include:

1. Waste Heat Utilization: This study innovatively explores the use of waste heat from GTCC power plants. By channelling the exhaust gases from the HRSG unit to power the MSF desalination unit, the system maximizes energy efficiency and reduces fuel consumption. This approach helps mitigate greenhouse gas emissions and aligns with sustainable energy practices.
2. Hybrid Desalination Approach: Combining MSF and RO technologies leverages the strengths of both methods. MSF processes offer high reliability and capacity, while RO processes require significantly less energy. The hybrid system aims to provide a robust and efficient solution for freshwater production in regions with high salinity and energy scarcity.
3. Sensitivity-Based Analysis: The study employs a sensitivity-based approach to evaluate the impact of Port Sudan's weather conditions on the performance of the GTCC-MSF-RO unit. This comprehensive assessment considers factors such as ambient air

temperature, seawater temperature, and salinity, providing a holistic understanding of the system's operational viability throughout the year.

4. Thermo-Economic Simulation: A detailed simulation of the proposed cogeneration system is conducted using Aspen HYSYS 10, facilitating a thorough thermo-economic analysis. This simulation provides insights into the system's efficiency, freshwater production capacity, and economic feasibility, highlighting potential cost savings and environmental benefits.
5. Alignment with Sustainable Development Goals: This research directly contributes to the United Nations' Sustainable Development Goals by addressing the critical challenges of water scarcity and energy insecurity prevalent in the MENA region. Specifically, the proposed hybrid MSF-RO desalination system integrated with a GTCC power plant aligns with SDG 6 (Clean Water and Sanitation) and SDG 7 (Affordable and Clean Energy) through the efficient and sustainable production of both freshwater and electricity.

2. Process description and model simulation

This paper investigates the retrofitting of a hybrid MSF-RO desalination unit to an existing GTCC power plant in Port Sudan. Figure 1shows the simulation schematic of the proposed cogeneration plant in Aspen HYSYS 10. The combined powercycle plant contains a gas turbine cycle (G.T.E.), the HRSG unit and the steam turbine cycle (S.T.E.). A once-through MSF unit (MSF-OT in Figure 1) and a RO unit generate fresh water. The simulation of cogeneration scheme in Aspen HYSYS uses the Peng-Robinson-Stryjek-Vera's (PRSV) fluid package. In this section, the main units of the steady state process simulation model of the power and water cogeneration plant shown in Figure 1are presented. The Aspen HYSYS logical unit operations used are explained. The flow chart of the mathematical model is shown in Figure 2.

2.1. Gas turbine combined cycle

The unit's operation used to model the gas turbine cycle are an air compressor, a combustion chamber, a high-pressure and a low-pressure turbine. The combustion chamber is simulated using the conversion reactor in Aspen HYSYS. A set of conversion reactions Equations (1) – (8) describe Fuel combustion. The molar composition of the natural gas and the operating parameters of the air and seawater are given in **Error! Reference source not found.**.

Fuel gas undergoes combustion with compressed air within the combustion chamber, generating high-temperature exhaust gases. These gases initially expand through the high-pressure gas turbine (HPT), producing sufficient power to drive the compressor. Subsequently, the gases expand further in the low-pressure gas turbine (LPT), generating additional power (Fig. 1). The LPT exhaust gases, at a temperature of 550 °C, enter the heat recovery steam generator (HRSG) where they transfer heat to produce steam through the superheater, evaporator, and economizer sections. Notably, instead of being released to the atmosphere, the exhaust gases exiting the economizer are directed to the brine heater of the osmotic turbine multi-stage flash (MSF-OT) desalination unit. The compressor inlet air temperature is subject to variations corresponding to the ambient conditions in Port Sudan, as detailed in Table 2.

$$CH_4 + 2(O_2 + 3.76N_2) \rightarrow CO_2 + 2H_2O + 3.76 \times 2N_2 \quad (1)$$

$$C_2H_6 + 3.5(O_2 + 3.76N_2) \rightarrow 2CO_2 + 3H_2O + 3.76 \times 3.5N_2 \quad (2)$$

$$C_3H_8 + 5(O_2 + 3.76N_2) \rightarrow 3CO_2 + 4H_2O + 3.76 \times 5N_2 \quad (3)$$

$$i - C_4H_{10} + 6.5(O_2 + 3.76N_2) \rightarrow 4CO_2 + 5H_2O + 3.76 \times 6.5N_2 \quad (4)$$

$$n - C_4H_{10} + 6.5(O_2 + 3.76N_2) \rightarrow 4CO_2 + 5H_2O + 3.76 \times 6.5N_2 \quad (5)$$

$$i - C_5H_{12} + 8(O_2 + 3.76N_2) \rightarrow 5CO_2 + 6H_2O + 3.76 \times 8N_2 \quad (6)$$

$$n - C_5H_{12} + 8(O_2 + 3.76N_2) \rightarrow 5CO_2 + 6H_2O + 3.76 \times 8N_2 \quad (7)$$

$$n - C_6H_{14} + 9.5(O_2 + 3.76N_2) \rightarrow 6CO_2 + 7H_2O + 3.76 \times 9.5N_2 \quad (8)$$

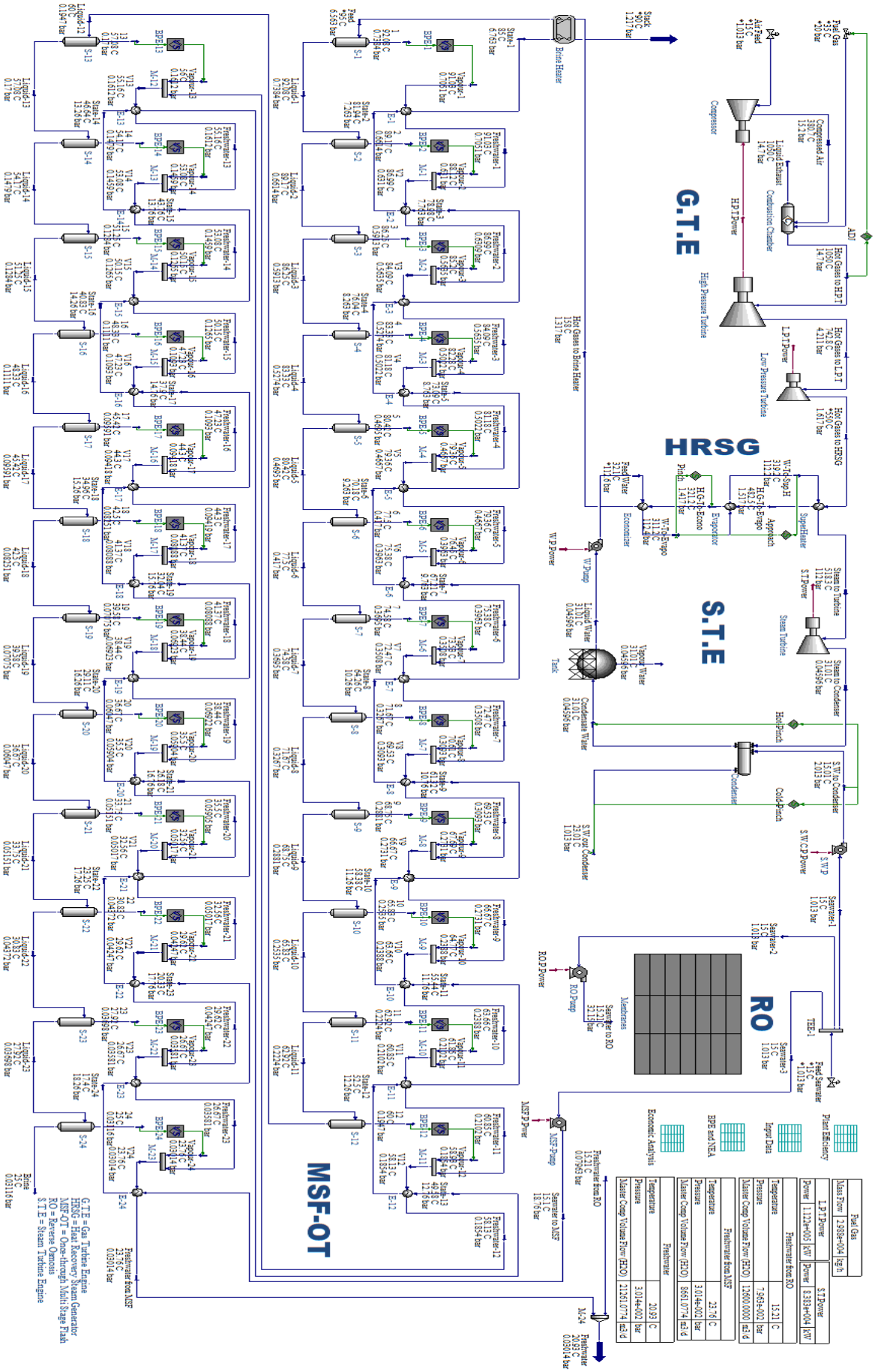

Figure 1. Schematic of proposed of CCPP coupled with the MSF-RO desalination unit.

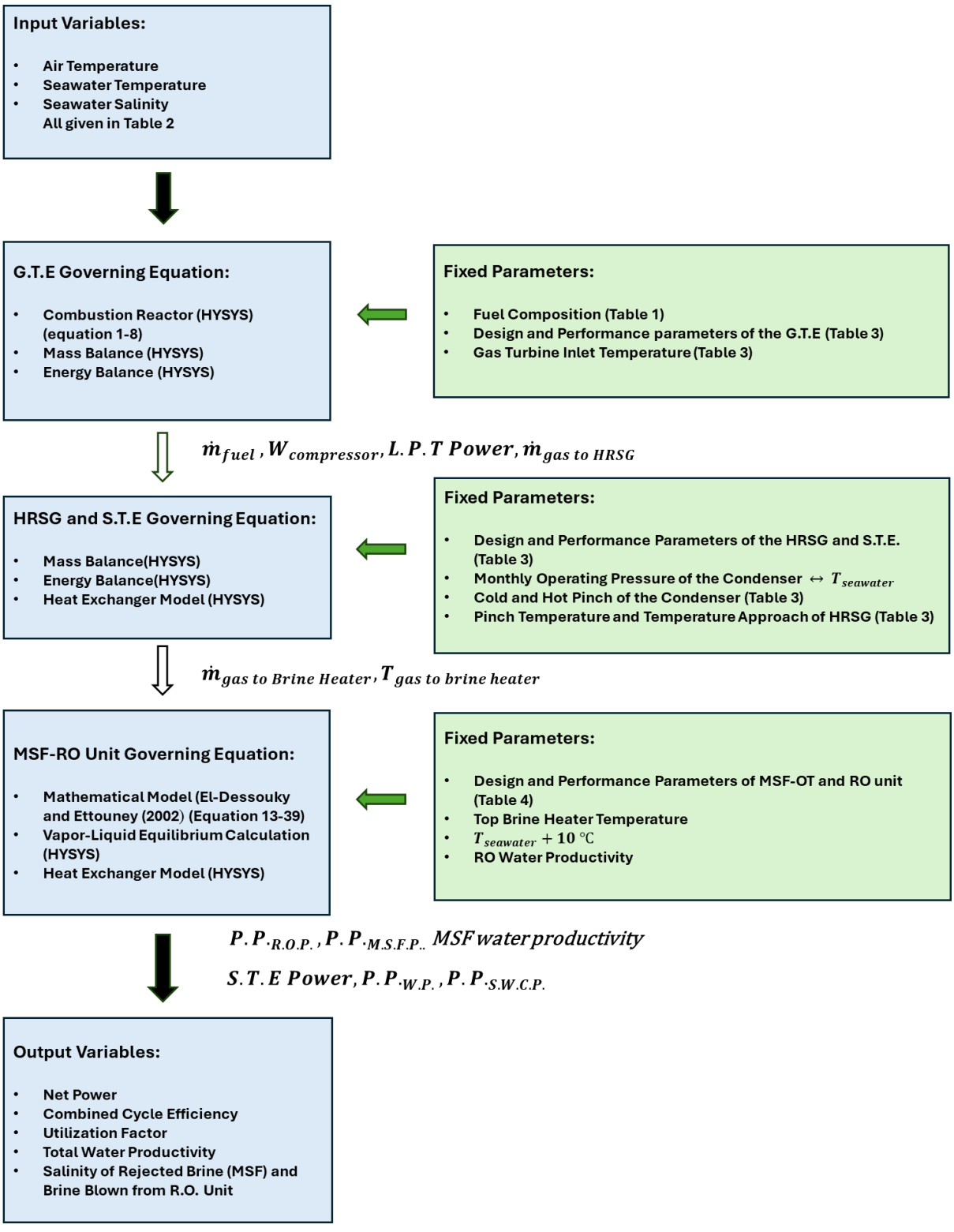

Figure 2. Flow chart showing the model of the proposed GTCC-MSF-RO system.

Table 1. System's input operating conditions.

Parameter	Symbol	The value	Unit
Fuel- Natural gas	Temperature	35	℃
	Pressure	20	bar
Fuel composition	Methane(CH_4)	98.000	%
	Ethane (C_2H_6)	00.253	%
	Propane (C_3H_8)	00.060	%
	i-Butane (C_4H_{10})	00.020	%
	n-Butane (C_4H_{10})	00.008	%
	i-Pentane (C_5H_{12})	00.007	%
	n-Pentane (C_5H_{12})	00.002	%
	n-Hexane (C_6H_{14})	00.020	%
	Nitrogen (N_2)	01.500	%
	Carbon dioxide (CO_2)	00.130	%
Air	Temperature	Monthly average	℃
	Pressure	1.01325	bar
	Mass flow	1.743251×10^6	kg. $(h)^{-1}$
Seawater	Temperature	Monthly average	℃
	Pressure	1.01325	bar
	Salinity	Monthly average	%

Table 2. Environmental input parameters in Port Sudan.

Months	Jan	Feb	Mar	Apr	May	Jun	Jul	Aug	Sep	Oct	Nov	Dec
Daytime temp (℃) **[48]**	28	28	30	35	37	40	43	43	39	32	30	28
Night-time temp (℃) **[48]**	21	21	22	27	30	32	34	35	32	29	28	24
Ave seawater temp (℃) **[49]**	26.78	25.28	25.56	26.89	26.44	27.5	27.78	27.94	30.94	30.61	29.78	27.89
Seawater salinity (%) **[49]**	3.9750	3.9577	3.9481	3.8769	3.8962	3.8750	3.9058	3.9038	3.9462	3.9269	3.9615	3.9712

The mass flow rate of air is 1.743251×10^6kg/h in all the simulations. Aspen HYSYS adjust operation (ADJ in Figure 1) is used to perform the iterations required to calculate the changes in fuel mass flow rate in response to seasonal variation in ambient air temperature. This approach mimics the fuel flow control (FFC) operating strategy used in GTCC. The target is to maintain the gas turbine inlet temperature (TIT) at 1050°C. Monthly values of fuel flow rate (kg/h), compressor power (MW), gas turbine power and mass flowrate of hot gases flowing to the HRSG are calculated using the G.T.E. cycle simulation model.

In this study, the HSRG unit is comprised of three shell and tube heat exchangers each representing the Economizer, Evaporator and Super-Heater, respectively. This unit is the connection between the G.T.E. and the S.T.E. cycles.

The steam turbine generates power by steam produced in the HRSG unit. Condensed steam turbine exhaust undergoes a phase change in the condenser. Condensed water is pumped from the storage tank to the economizer section of the HRSG unit. Feed water is heated gradually by the heat energy of the exhaust gases as described above. A shell-and-tube heat exchanger unit simulates the condenser. In the S.T.E. cycle, monthly variations of the temperature and salinity of seawater in Port Sudan affect the operating (saturation) pressure of the condenser.

The set function (Cold-Pinch and Hot-Pinch in Figure 1) in Aspen HYSYS implements the temperature differences between streams at the cold end and hot end of the condenser respectively. The cold pinch value is the difference between cooling seawater temperature (S.W. to Condenser stream) and the temperature of condensed water (Condensate water stream). The hot pinch value is the difference between the temperature of the steam turbine exhaust (Steam to Condenser stream) and seawater leaving the condenser (S.W. out Condenser stream). The cold and hot pinch values of the condenser are set at 16 °C and 8 °C respectively.

Monthly changes in the mass flow rate of hot gases fed to the HRSG (Super-Heater) unit and the temperature of water condensate (Feed Water stream) flowing from the S.T.E. cycle affect the heat balance in the HRSG unit. Optimal operation of the HRSG units is guaranteed by maintaining the pinch temperature and approach temperature of the HRSG at 10°C and 8°C, respectively. The pinch temperature is the difference between the temperature of exhaust gases that exit the evaporator section, and the temperature of water stream fed to the evaporator (W. to Evaporator stream). The temperature approach is the difference between the temperature of the water stream fed to the evaporator (W. to Evaporator stream) and the temperature of the saturated steam leaving the evaporator (W-To-SupH stream). The set function (Pinch and Approach in Figure 1) in Aspen HYSYS implements the temperature differences between streams as explained above. The design parameters of the GTCC plant are given in Table 3.

Table 3. Design parameters and performance of the GTCC plant.

Parameter	Symbol	The value	Unit
Centrifugal compressor	Adiabatic efficiency	88	%
	Pressure Ratio	15	--
	c_{11}	44.71	$\$.(\mathrm{kg.s})^{-1}$
	c_{12}	0.95	
Reactor	Efficiency	99.9	%
	Losses pressure	50	kPa
	c_{21}	28.98	$\$.(\mathrm{kg.s})^{-1}$
	c_{22}	0.015	K^{-1}
	c_{23}	1540	K
High& Low-pressure gasTurbine	Adiabatic efficiency	90	%
	Adiabatic efficiency	90	%
	c_{31}	301.45	$\$.(\mathrm{kg.s})^{-1}$
	c_{32}	0.94	
	c_{33}	0.025	K^{-1}
HRSG	HRSG pressure	112	bar
	Losses pressure in the-shell	10	kPa
	Losses pressure in the-tube	20	kPa
	Pinch-point temperature	10	℃
	Approach temperature	8	℃
	c_{41}	6570	
	c_{42}	21276	
	c_{43}	1184.8	
Steam turbine	Steam mass flow	2.4029×10^{5}	$\mathrm{kg.(h)}^{-1}$
	Adiabatic efficiency	90	%
	c_{51}	3880.5	$\$.(\mathrm{kW})^{-0.7}$
Condenser	Hot pinch temperature	16	℃
	Cold pinch temperature	8	℃
	Losses pressure in the-shell	100	kPa
	c_{71}	1773	
Steam cycle pump	Adiabatic efficiency	75	%
	Pressure	112.6	bar
	c_{61}	705.48	$\$.(\mathrm{kg.s})^{-1}$
Steam condenser pump	Adiabatic efficiency	75	%
	Pressure ratio	1.987	
	c_{61}	705.48	$\$.(\mathrm{kg.s})^{-1}$
Economic parameters	Interest rate (i)	10	%
	Plant life (q)	20	year
	Time of operation (Y)	335	(day/year)
	Price of fuel (c_{fuel})	3.30	$\$.(\mathrm{GJ})^{-1}$
	Price of selling electricity (c_{el})	0.044	$\$.(\mathrm{kWh})^{-1}$
	Price of selling water (c_w)	0.1	$\$.(\mathrm{m}^3)^{-1}$
	Unit damage cost for NO_X emission (c_{NOx})	6.85	$\$.(\mathrm{kgNO_X})^{-1}$
	Coefficient of M&O cost (β)	0.06	

In the simulation presented in this study, changes in the temperature of the steam stream leaving the Super-Heater end of the HRSG (Steam to Turbine stream) and mass flow rate and temperature of HRSG exhaust gas stream (Hot Gases to Brine Heater stream) at the Economizer end mirrors the effect of weather conditions on the G.T.E. and S.T.E. cycles. Therefore, the effect of seasonal variations of ambient air temperature, seawater temperature and seawater salinity on the net power of the GTCC cycle and waste energy available to power the MSF unit (MSF thermal power) is determined. Monthly variations of fuelflow rate(kg/h), air mass density($\mathrm{kg/m^3}$), air compressor power(MW), gas turbine power, steam turbine power(MW)are output variables of the power cycle simulation model.

The monthly net power output of the combined cycle is calculated from the steam turbine power (S.T. Power in Figure 1) and the gas turbine power(L.P.T. Power in Figure 1)after subtracting the monthly total pump power requirement of the plant as shown in Equation (9).

$$Net\ Power = L.P.T.Power + S.T.Power - Total\ Pump\ Power \quad (9)$$

The total pump power is the summation of power required to circulate water from the condenser to the HRSG unit (W.P. Power in Figure 1), to feed seawater to the condenser (S.W.C.P. Power in Figure 1) and to the RO (R.O.P. Power in Figure 1) and MSF units (MSF.P. Power in Figure 1). These are calculated using the simulation model output energy streams as shown in Equation(10).

$$Total\ Pump\ Power = P.P._{W.P.} + P.P._{S.W.C.P.} + P.P._{R.O.P.} + P.P._{M.S.F.P.} \quad (10)$$

The combined cycle efficiency is expressed by:

$$\eta_{CC} = \frac{NetPower}{\dot{m}_g LHV_{NG}} \quad (11)$$

The utilization factor (UF)[21]is obtained as follows:

$$UF = \frac{Net\ Power + W_{de}}{\dot{m}_g LHV_{NG}} \quad (12)$$

2.2. Desalination plant

The MSF-OT desalination unit is composed of a top brine heater (Brine heater in Figure 1), 24 desalination stages and the bottom feed water heater (E_{24} in Figure 1).Each stage (i) is simulated using a vapor-liquid separator (S_i) and a shell and tube heat exchanger (E_i). The Separator represents the flashing chamber while the shell and tube heat exchanger represent the condenser. In the heat exchanger, the latent heat of the condensed vapor leaving stage (i) heats the seawater coming from the stage $(i+1)$.The brine heater increases the temperature of seawater exiting the condenser of the first stage (E_1 in Figure 1), from$(T_1)$to the top brine heater temperature (T_b). The heating medium is the exhaust gases of the HRSG unit. The stack gas temperature is fixed at 90°C.

The basic mathematical model byEl-Dessouky and Ettouney [50]was used to estimate the temperature profile of MSF flashing stages as described below. The pressure in each chamber was calculated based on the saturation temperature of each stage. Successive pressure-drop from one stage to the next drives brine flow from one stage to the next. The simulation model output are the mass flow rate of seawaterand the MSF-water productivity (m^3/day). Both vary monthly in response to changes in feed seawater temperature (T_f) and salinity shown in Table 2. In addition, fluctuations in the energy of the exhaust gases of the HRSG, the main heat source of the brine heater, affect monthly total freshwater productivity.

The temperature profile in the MSF-OT unit is defined in terms of the temperature of the brine leaving the preheater (top brine temperature: T_b), the brine leaving the last stage (T_{24}) and the feed seawater temperature (T_f).The top brine heater was set equal to 95 °C. T_f varies according to the monthly weather data given in Table 2. The temperature of the rejected brineT_{24} (leaving the last stage) is set equal to 10°C higher than (T_f).The temperature difference between the top brine heater temperature (T_b =95°C) and the temperature of the brine leaving the last stage in this module (T_{24}) is the evaporation range $(T_b - T_{24})$Alhazmy [51]. Allowing the rejected brine temperature to vary with the seasonal changes of the seawater feed temperature is expected to enhance the production rate of fresh water by the MSF unit especially in cold seasons. The stage temperature drop (ΔT) is assumed to be equal and is obtained from the relation:

$$\Delta T = \frac{(T_b - T_{24})}{24} \quad (13)$$

The temperature of the flashing stage i, is equal to:

$$T_i = (T_b - i \times \Delta T) \quad (14)$$

The input parameters of the MSF-OT units are given in Table 4and are inserted as a SPREAD SHEET (Input Data) in Aspen HYSYS. In the simulation model the temperature of the vapor (T_{vi})leaving the vapor-liquid separator was corrected for to thermodynamic losses caused by boiling point elevation(BPE) and the non-equilibrium allowance(NEA)[50, 52]. The vapor condensation temperature for each stage(T_{vi}) is calculated using equations (15) – (25).

$$T_{v_i} = T_i - BPE_i - NEA_i - \Delta T_{dim_i} \quad (15)$$

The temperature drop in the demister (ΔT_{dim}) is assumed to be negligible compared to (BPE) and (NEA). The values of B and C in the correlation for the boiling point elevation are:

$$BPE_i = X_i[B + (X_i \times C)] \times 10^{-3} \quad (16)$$

$$B = \left[6.71 + 6.34 \times 10^{-3} \times (T_i) + 9.74 \times 10^{-5} \times \left(T_i{}^2\right)\right] \times 10^{-3} \quad (17)$$

$$C = \left[22.238 + 9.59 \times 10^{-3} \times (T_i) + 9.42 \times 10^{-5} \times \left(T_i{}^2\right)\right] \times 10^{-8} \quad (18)$$

where (T) is the temperature and (X) is the salt weight percentage. The above equation is valid over the following ranges: $1 \le X \le 16\%, 10 \le T \le 180$ ℃.

Lior [53]established correlations to account for non-equilibrium conditions within the MSF system. These equations provide values for the non-equilibrium allowance as a function of brine temperature, gate height, brine flow rate per unit chamber width, and stage temperature drop.

$$(NEA)_{10} = (0.9784)^{T_i}(15.7378)^{H}(1.3777)^{V_b \times 10^{-6}} \quad (19)$$

$$NEA = \frac{(NEA)_{10}}{(0.5\Delta T + NEA_{10})^{0.3281L}(0.5\Delta T + NEA_{10})} \quad (20)$$

Equation(19) is valid for 10 ft stage length and Equation(20) is applicable for stages of any other lengths. (T_i) is the stage temperature, (H) is the height of the brine pool, $(V_b)$is the brine flow rate per unit length of the chamber width, and $\Delta T$is the stage temperature drop.The gate height $(GH)$is obtained in terms of the stage pressure drop (ΔP), the brine density (ρ_b), the weir friction coefficient (C_d), the stage width (SW), and the feed flow rate$(\dot{m}_f)$. For stage i the gate height is

$$GH_i = \left(\dot{m}_f - \sum_{j=1}^{i-1} D_j\right) \times \left(2\rho_{b_j}\Delta P_i\right)^{(-0.5)} / (C_d.SW) \quad (21)$$

The brine pool height is set higher than the gate height by 0.2 m.

$$H_i = 0.2 + GH_i \quad (22)$$

$$\Delta P_i = P_i + P_{i+1} \quad (23)$$

$$SW = \frac{M_f}{V_b} \quad (24)$$

where (P_i) and (P_{i+1}) are the pressures in stages $(i)$and $(i+1)$, and $(V_b)$is the brine mass velocity per chamber width. The length of the last stage is determined as a function of the vapor flow rate (D_n), the vapor density (ρ_{V_n}), the vapor allowable velocity (V_{V_n}), and the stage width(SW).

$$L = \frac{D_n}{\rho_{V_n} V_{V_n} SW} \quad (25)$$

The temperature correction is implemented in the simulation using the virtual stream extension (BPE) shown in Figure 1.Compared to previous studies using Aspen HYSYS[43, 47], this work presents the most

comprehensive HYSYS simulation of once-through multi-stage desalination process published to date.

The RO unit was modeled using the mathematical model by El-Dessouky and Ettouney [50]. The set of equations (Equations (26) – (38)) are shown below.

The feed flow rate $(\dot{m}_f)$ based on recovery ratio (RR) and distillate flow rate $(\dot{m}_d)$ is:

$$\dot{m}_f = \frac{\dot{m}_d}{RR} \quad (26)$$

The distillate product salt concentration (X_d)

$$X_d = X_f \times (1 - SR) \quad (27)$$

where $(X_f)$is the feed flow rate salt concentration, and (SR) is the salt rejection percentage; and the rejected brine is found from:

$$\dot{m}_b = \dot{m}_f - \dot{m}_d \quad (28)$$

The rejected salt concentration is estimated by:

$$X_b = \frac{\dot{m}_f \times X_f - \dot{m}_d \times X_d}{\dot{m}_b} \quad (29)$$

The average salt concentration is estimated as:

$$X_{av} = \frac{\dot{m}_f \times X_f - \dot{m}_b \times X_b}{\dot{m}_f + \dot{m}_b} \quad (30)$$

The temperature correction factor (TFC) is found by the relation [54, 55]

$$TFC = \exp\left[2700 \times \left(\frac{1}{273+T} - \frac{1}{298}\right)\right] \quad (31)$$

The membrane water permeability (k_w)[54, 55]

$$k_w = 6.84 \times 10^{-8} \times \left[\frac{18.6865 - (0.177 \times X_b)}{(T+273)}\right] \quad (32)$$

The salt permeability (k_s) is:

$$k_s = FF \times TCF \times 4.72 \times 10^{-7} \times \left[0.06201 - \left(5.31 \times 10^{-5} \times (T+273)\right)\right] \quad (33)$$

where the membrane fouling factor, denoted by (FF), influences the system's performance. Osmotic pressure calculations for the feed, brine, and distillate product sides were determined using the following equations:

$$\pi_f = 75.84 \times X_f \quad (34)$$

$$\pi_b = 75.84 \times X_b \quad (35)$$

$$\pi_d = 75.84 \times X_d \quad (36)$$

The average osmotic pressure on the feed side and the net osmotic pressure across the membrane are found as follows:

$$\pi_{av} = 0.5 \times (\pi_f + \pi_b) \quad (37)$$

$$\Delta\pi = \pi_{av} - \pi_d \quad (38)$$

The net pressure difference across the membrane Equation (39) and the required high pressure pump power input to the RO Equation (40) was modelled using Moharram, et al. [44] as;

$$\Delta P = \left(\frac{\dot{m}_d}{3600 \times TCF \times FF \times A_e \times n_e \times n_v \times k_w}\right) + \Delta\pi \quad (39)$$

$$P.P._{R.O.} = \frac{1000 \times \dot{m}_f \times \Delta P}{3600 \times \rho_f \times \eta_p} \quad (40)$$

where (A_e) is the element area, (n_e) is number of membrane elements, (n_v) is the number of pressure vessels, (ρ_f) the feed is flow rate density, and (η_p) is the driving pump mechanical efficiency.

The RO unit was included in the simulation using the SPREADSHEET option (Membranes shown in Figure 1). The water production target of the RO unit (RO-water productivity stream) is constant and equals 12,600 cubic metres per day. The effect of monthly variations of seawater temperature and salinity in Port Sudan on the power requirement of the high-pressure pump of the RO unit $(P.P._{R.O.})$ are considered.

In the MSF-OT and RO sections, seawater usually enters at variable temperatures according to the monthly average seawater temperature of Port Sudan (Table 2) , with the input data for the MSF-OT and RO desalination plants provided in Table 4.

The process simulation model of the power plant was verified by comparison with a reference case Bălănescu and Homutescu [56]. Details of the model validation are described in the supplementary material (SM) section. The simulation of MSF-OT and RO units were also validated using published dataEl-Dessouky and Ettouney [50]and the corresponding results are shown in the SM section. The validated model of the combined power and desalination plant is run using weather conditions (Table 2) and the input data of the power plant of Port Sudan (Table 3). Because of the low moisture content, the effect of air moisture content on performance of the plant is assumed negligible Liu and Karimi [57].

2.3. Economic analysis

Simulation results of proposed scheme were used to perform an economic analysis as previously described by[37]. Values of the economic parameters are given in and Table 4 and Table 4.

Calculation of the total annual cost (TAC) included the annual investment cost $(\dot{C}_{ac})$, annual maintenance and operating costs $(\dot{C}_{M\&O})$ and NO_Xemission penalty cost $(\dot{C}_{NO_X})$ as shown in equation (41)[37].

$$\text{TAC} = \dot{C}_{ac} + \dot{C}_{M\&O} + \dot{C}_{NO_X} \quad (41)$$

The investment cost (C_{In})includes all costs associated with establishing a facility. This cost falls into the direct (C_{di}) and indirect cost (C_{id})categories[37, 58, 59] as presented in equation(42).

$$C_{In} = C_{di} + C_{id} \quad (42)$$

Direct investment expenses include major and auxiliary equipment, site construction, and land costs.

$$C_{di} = C_{la} + C_{eq} + C_{sd} \quad (43)$$

Table 4. Input data of MSF and RO desalination plant proposed.

Parameter	The value	Unit
MSF- type	**Once through MSF**	
Number of stages (n)	24	Stage
Top brine temperature	95	℃
Hot pinch temperature	10	℃
Losses pressure in the evaporates-shell	50	kPa
Losses pressure in the brine heater-shell	10	kPa
Losses pressure in the brine heater-tube	20	kPa
Vapor velocity in the last stage $\boldsymbol{V_{V_{24}}}$	6	$\mathrm{m.(s)^{-1}}$
Brine mass flow rate per stage width $\boldsymbol{V_b}$	180	$\mathrm{kg.(m.s)^{-1}}$
Weir friction coefficient $\boldsymbol{C_d}$	0.5	--
Pump pressure ratio	18.52	--
Brine heater heat transfer area $\boldsymbol{A_b}$	100	$\mathrm{m^2}$
Condenser heat transfer area $\boldsymbol{A_{con}}$	60.32	$\mathrm{m^2}$
$\boldsymbol{c_{81}}$	6000	--
RO membrane type	**SW30HR-380**	
Membrane fouling factor	85	%
Area	35	$\mathrm{m^2}$
Permeate flow rate	20	$\mathrm{m^3/day}$
Number of membrane elements	7	Modules
Number of pressure vessels	90	Vessels
Recovery ratio	30	%
Salt rejection	99.7	%
Pump efficiency	75	%
Inflation factor$\boldsymbol{\xi}$	1.399	
$\boldsymbol{c_{91}}$	7846	$
$\boldsymbol{c_{92}}$	996	
$\boldsymbol{c_{93}}$	393000	
$\boldsymbol{c_{94}}$	701.19	

In the current study, the land cost (C_{la}) is not considered due to land availability. Mass flow rates, temperature and pressure values of the process streams required in equations (44) – (53) to calculate the processing equipment costs (C_{eq}) are extracted from simulation results. Plant Equipment included the air compressor (AC), the combustion chamber (CC), the gas turbine (GT), the HRSG, the steam turbine (ST), the pumps (P), steam condenser (CON), the MSF desalination unit (MSF) and the RO desalination unit (RO).

$$\mathrm{C_{eq}} = \mathrm{C_{AC}} + \mathrm{C_{CC}} + \mathrm{C_{GT}} + \mathrm{C_{HRSG}} + \mathrm{C_{ST}} + \mathrm{C_P} + \mathrm{C_{CON}} + \mathrm{C_{MSF}} + \mathrm{C_{RO}} \tag{44}$$

Air compressor[60, 61]:

$$\mathrm{C_{AC}} = \mathrm{c_{11}} \times \dot{\mathrm{m}}_{\mathrm{air}} \times \frac{1}{[\mathrm{c_{12}} - \eta_{\mathrm{s,C}}]} \times \mathrm{r_p} \times \ln \mathrm{r_p} \tag{45}$$

Combustion chamber[60, 61]:

$$C_{CC} = c_{21} \times \dot{m}_{air} \times \left(1 + e^{c_{22}\cdot(T_{out}-c_{23})}\right) \times \frac{1}{\left[0.995 - \frac{p_{out}}{p_{in}}\right]} \quad (46)$$

Gas turbine[60]:

$$C_{GT} = c_{31} \times \dot{m}_g \times \frac{1}{\left[c_{32} - \eta_{s,GT}\right]} \times \ln\frac{p_{in}}{p_{out}}\left(1 + e^{c_{33}\times(T_{in}-1570K)}\right) \quad (47)$$

Heat recovery steam generator[61, 62]:

$$C_{HRSG} = c_{41} \times \left[\left(\frac{Q_{EC}}{\Delta T_{EC}}\right)^{0.8} + \left(\frac{Q_{EV}}{\Delta T_{EV}}\right)^{0.8} + \left(\frac{Q_{SH}}{\Delta T_{SH}}\right)^{0.8}\right] + c_{42} \times \dot{m}_w + c_{43} \times {\dot{m}_g}^{1.2} \quad (48)$$

Steam turbine[60]:

$$C_{ST} = c_{51} \times {P_{ST}}^{0.7} \times \left[1 + \left(\frac{0.05}{(1 - \eta_{s,ST})}\right)^3\right] \times \left[1 + 5 \times \exp\left(\frac{(T_{in} - 866K)}{10.42K}\right)\right] \quad (49)$$

Water pumps [60]:

$$C_P = c_{61} \times {P_P}^{0.71} \times \left[1 + \frac{0.2}{(1 - \eta_{s,P})}\right] \quad (50)$$

Condenser[63]:

$$C_{CON} = c_{71} \times \dot{m}_s \quad (51)$$

Multi stage flash [11, 50]:

$$C_{MSF} = \frac{0.096 \times c_{81} \times (A_b + 24 \times A_c)}{(\dot{m}_{de})^{0.27}} \quad (52)$$

Reverse osmosis:[61, 64, 65]

$$C_{RO} = c_{91} \times NO_{membranes} + c_{92} \times \xi \times \left(\frac{\dot{m}_{RO}}{\rho} \times 24 \times 3600\right)^{0.8} + c_{93} \times \xi + 14.5 \times c_{94} \times P_{RO} \quad (53)$$

Site development cost (C_{sd}) is estimated using equation (54)[37].

$$C_{sd} = 0.2 \times C_{eq} \quad (54)$$

The indirect investment cost (C_{id}) includes freight cost (C_{fr}), construction overhead cost (C_{co}), owner's cost (C_{ow}) and contingency cost (C_{cm}). Equations(55) – (59) present the calculation detail[58].

$$C_{id} = C_{fr} + C_{co} + C_{ow} + C_{cm} \quad (55)$$

$$C_{fr} = 0.05 \times C_d \quad (56)$$

$$C_{co} = 0.15 \times C_{eq} \quad (57)$$

$$C_{ow} = 0.1 \times C_{eq} \quad (58)$$

$$C_{cm} = 0.1 \times C_d \quad (59)$$

To determine the annual cost, the investment cost should be amortized using the capital recovery factor (CRF)[37] calculated using equations(60) and (61), respectively.

$$\dot{C}_{ac} = CRF \times C_{In} \quad (60)$$

$$CRF = \frac{i(1+i)^q}{(1+i)^q - 1} \quad (61)$$

where (i) is the interest rate and (q) is the plant lifetime. Interest rate and plant lifetime was set as 10% and 20 years, respectively.

Annual maintenance and operational costs $(\dot{C}_{M\&O})$are those expended following plant commissioning and during operation. The maintenance cost is calculated as a percentage of the annual investment cost $(\dot{C}_{ac})$. Monthly pump power requirement of the plant was subtracted the power produced by the GTCC plant as previously described in equation (9); therefore monthly operating cost include fuel costs presented in equation (62)[37].

$$\dot{C}_{M\&O} = \beta \times \dot{C}_{ac} + c_{fuel} \times LHV \times \dot{m}_{fuel} \times Y \times 24 \times 3600 \quad (62)$$

The annualNO_X emissions penalty cost ($\dot{C}_{NO_X}$) was calculated by taking into account milligrams of NO_X in 1 kg of combustion product ($\dot{m}_{product}$) using equation (63)[37].

$$\dot{C}_{NO_X} = c_{NO_X} \times \dot{m}_{product} \times 150 \times 10^{-6} \times Y \times 24 \times 3600 \quad (63)$$

The annual income $(\dot{S})$received from selling the fresh water and electricity is obtained by:

$$\dot{S} = \left(W_{Net\ power} \times Y \times c_{el} \times 24\right) + (\dot{m}_d \times Y \times c_w \times 24 \times 3.6) \quad (64)$$

Where (c_{el}) and (c_w) is the electricity and water selling prices, respectively.

The payback period (pp) was calculated by setting the Net Present Worth (NPW) and Net Future Worth (NFW)equal to zero in equations(65) and (66), respectively[37].

$$NPW = -C_{In} - \dot{C}_{M\&O}\left[\frac{(1+i)^{pp} - 1}{i(1+i)^{pp}}\right] + \dot{S}\left[\frac{(1+i)^{pp} - 1}{i(1+i)^{pp}}\right] \quad (65)$$

$$NFW = -C_{In}(1+i)^{pp} - \dot{C}_{M\&O}\left[\frac{(1+i)^{pp} - 1}{i}\right] + \dot{S}\left[\frac{(1+i)^{pp} - 1}{i}\right] \quad (66)$$

3. Results and discussion

3.1. Validation of the simulation model

Increased water scarcity, energy poverty and ongoing reduction of fossil-fuel consumption is increasing the need to maximize energy recovery of waste streams before their rejection to the environment.

Techno-economic evaluation of power-water cogenerating systems have contributed to the investigation of different dual-purpose plant configurations. The HYSYS simulation of the GTCC power cycle was verified by comparison to a reference case Bălănescu and Homutescu [56]. The process flow diagram of the reference power plant and the corresponding HYSYS simulation schematic is shown inFig.SM 1. The process parameters of the Orenda OGT15000 gas turbine calculated by the HYSYS simulation were in good agreement with values as shown in Table SM 1.The flow diagram of the MSF-OT of the model and the performance characteristics of the desalination unit El-Dessouky and Ettouney [50] are shown in Figure SM 2 and Table SM 2, respectively.

The simulation results for the distillate flow rate, the steam flow rate, and the performance ratio are almost identical with the model output of the mathematical modelEl-Dessouky and Ettouney [50]. Error did not exceed 4.6%.A comparison of the values of distillate flow rate, brine flowrate and the salinity of the brine for each desalination stage is presented inFigure SM 3. Maximum error in distillate flowrate is in the first and final stages and does not exceed 3.6%. Compared to the reference case, the current model underestimates the brine flowrate in each stage by average 4.7%. The error of the salinity of the brine for each stage is very small 0.1% at the first stage and then diverges to reach highest value 1.8% at the last stage. The temperature profile of all the streams ofMSF unit in each stage (feed seawater, condensing vapor, and brine) agrees very well with the reference case as shown in Table SM 3.It is important to note that that the mathematical model by El-Dessouky and Ettouney [50]uses an approximate equation to calculate the performance ratio of the MSF-OTsystem (kg distillate/ kg steam). The latent heat of condensation used is based on an average stage temperature. In the simulation model performed in this study, the energy balance of the unit is based on a more accurate stage wise flashing evaporation phenomenon in the two-phase separator unit.

3.2. Results of thermodynamic analysis

The operating environment and designed conditions for power plants vary significantly based on their location, which affects their performance compared to the ideal conditions set by the International Organization for Standardization (ISO)[66-68] as show inTable 5.

Table 5. International Organization for Standardization (ISO) condition.

Parameter	The value	Unit
Dry ambient air temperature	15	℃
Relative humidity	60	%
Atmospheric pressure at the sea level	1.01325	bar
Seawater temperature	15	℃
Seawater salinity	35000	PPM

ISO provides standard conditions for a consistent basis of comparison, but real-world conditions often deviate from these standards. The design parameters for the simulation results of the GTCC-MSF-RO unit using ISO conditions are shown in Table 6.

The simulation of the GTCC-MSF-OR unit was performed using the input data of the power plant in Port Sudan and weather condition data (Table 2). The results of the simulation model of the integrated power and water generation plant show that it is possible to produce at least 7,624 m^3/day of freshwater using the waste energy of the exhaust gases of the HRSG. This constitutes 60% of the freshwater produced by the RO unit powered by electricity. The productivity of the MSF unit proposed in this study is comparable to the capacity of medium scale MSF unit.

It of great relevance to Sudan to retrofit an existing combined cycle power plant with a medium scale MSF unit powered by the waste heat of the power cycle. The results obtained contributes to ongoing research efforts aiming at producing freshwater using waste heat streams[46, 47, 69]or using solar energy systems[42-45].

The performance of the MSF unit was evaluated under different weather conditions. Ambient air temperature and seawater temperature in Port Sudan(shown in Table 2)record its lowest value in January, February, and December. The highest air temperature is in the summer months of July and August. Average seawater temperatures rise steadily and reach their maximum in the month of September. In this month and the following months, the difference between average air and average seawater temperatures is minimal.

Low ambient air temperature and low seawater temperature in the winter months of December, January and February are optimal for power generation as shown in Fig. In this season, the maximum monthly fuel consumption rate (Fig(a))is recorded. Due to the high air density values(Fig(b)) and consequently low air compressor power (Fig(c)) required, maximum power is generated by the gas(Fig(d)) and steam(Fig (e)) turbines. After subtracting the steam cycle pump requirement (Fig (f)),the net power output of plant is 177.5MW (Fig(g)). Combined cycle efficiency (45.84%) (Fig(h)) and utilization factor (55.72%)(Fig(i)) are at their highest monthly value.

Table 6. Performance results of the CCGT plant and MSF-RO desalinations operating in ISO condition.

Parameter	The value	Unit
Fuel flow	29878.76	kg. $(h)^{-1}$
Air mass density	1.22100	kg/m^3
Net power	190.542	MW
Compressor power	185.547	MW
Gas turbine power	297.713	MW
Steam turbine power	83.828	MW
Steam cycle pump power	0.999	MW
Efficiency	47.29	%
Utilization factor	56.16	%
Steam turbine temperature	518.30	℃
Steam condenser temperature	31.01	℃
MSF-rejected brine temperature	25.00	℃
MSF-thermal power	128.562	GW/h
RO-electrical power	2.0837	MW
MSF- water productivity	8661.07	m^3/day
RO-water productivity	12600.00	m^3/day
Total water productivity	21261.07	m^3/day
MSF- feed seawater	68135.39	m^3/day
RO- feed seawater	42000.00	m^3/day
MSF-salinity	40250.66	PPM
RO-salinity	49955.00	PPM

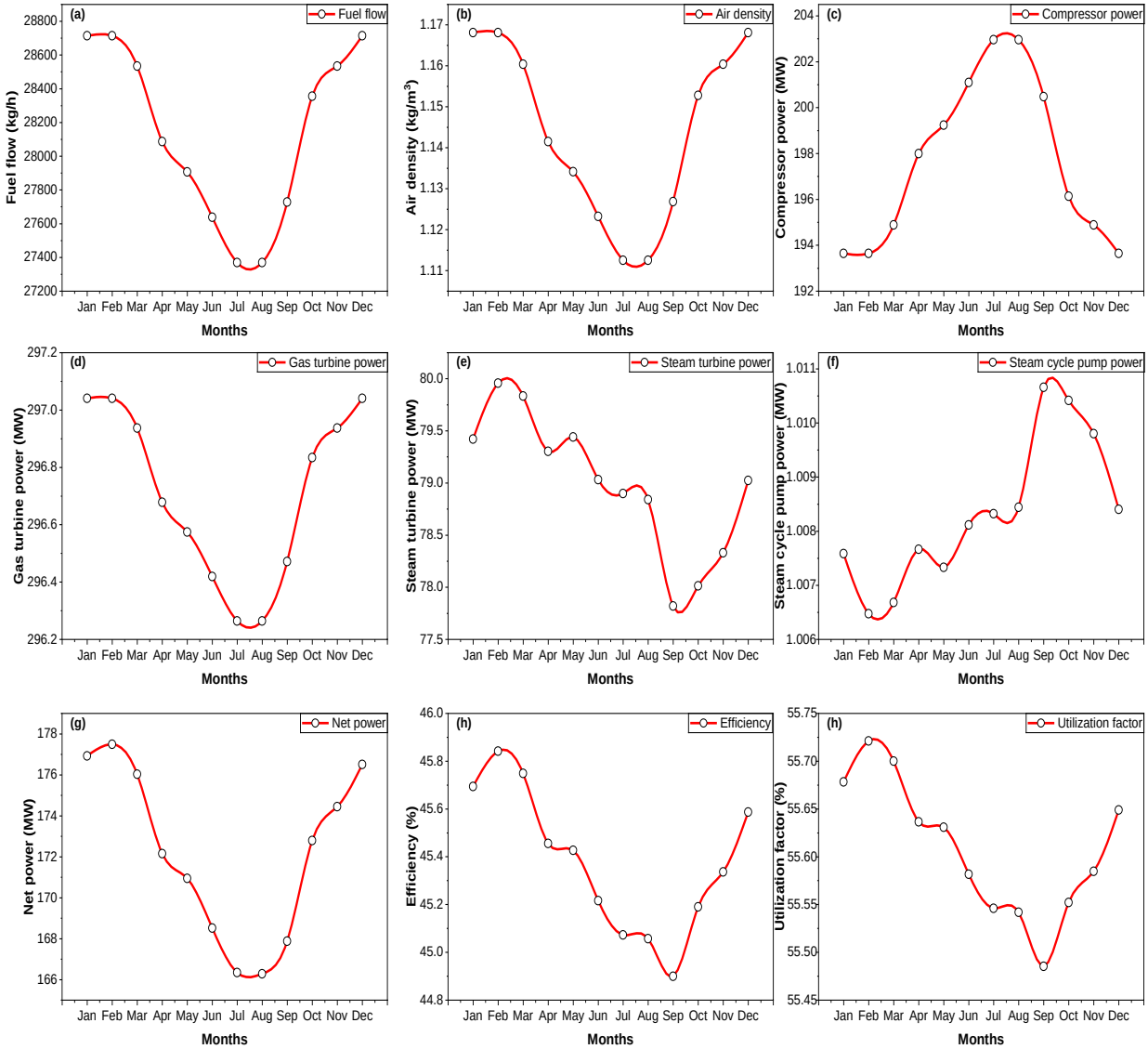

Figure 3. Monthly variation in the performance parameters of the power cycle in response to weather conditions. (a) fuel flow. (b) air mass density. (c) compressor power. (d) gas turbine power. (e) steam turbine power. (f) steam cycle pump power. (g) net power. (h) efficiency. (i) utilization factor.

In winter the temperature of the steam cycle condenser (Fig(a)) and the corresponding saturation pressure are low due to the cold sea water temperature. The steam turbine temperature is the highest relative to the rest of the year (Fig (b)).The mass flow rate and temperature of HRSG exhaust gas stream obtained in the winter month are used to determine MSF thermal power (Fig(c)).

According to the simulation results of the combined cycle, it was likely to expect that freshwater production would be minimal in these winter months, because both the MSF-thermal power (Fig(c)) and the temperature of the brine heater (Fig(d)) are at their lowest values. Surprisingly, the thermal desalination unit produces 8,025m^3/day, which is the highest monthly value (Fig(e)). The result can be explained by the fact that the evaporation range of the MSF unit has a maximum value of 58.22°C in February. The span along which evaporation occurs is maximum as confirmed by the low temperature of the rejected brine (Fig(f)).The findings of this comprehensive simulation model imply that the evaporation range of an MSF unit has a stronger effect on freshwater productivity than the thermal energy supplied to the brine heater. The dominating effect of evaporation range is mirrored by research interest in defining temperature control strategies for the different seasons [70]and propose operating strategies [9, 51]of MSF units.

Changes in the electrical power of the RO unit (Fig (g)) is primarily due to fluctuations in seawater salinity, which has its highest and lowest value in January (3.9750%) and June (3.8750%), correspondingly. The pumping power varies to maintain water production at 12,600 m^3/day (Fig (h)) at constant seawater feed to the RO unit (42,000 m^3/day). In winter, total water production by the cogeneration plant is highest at 20,625 m^3/day (Fig (i)).

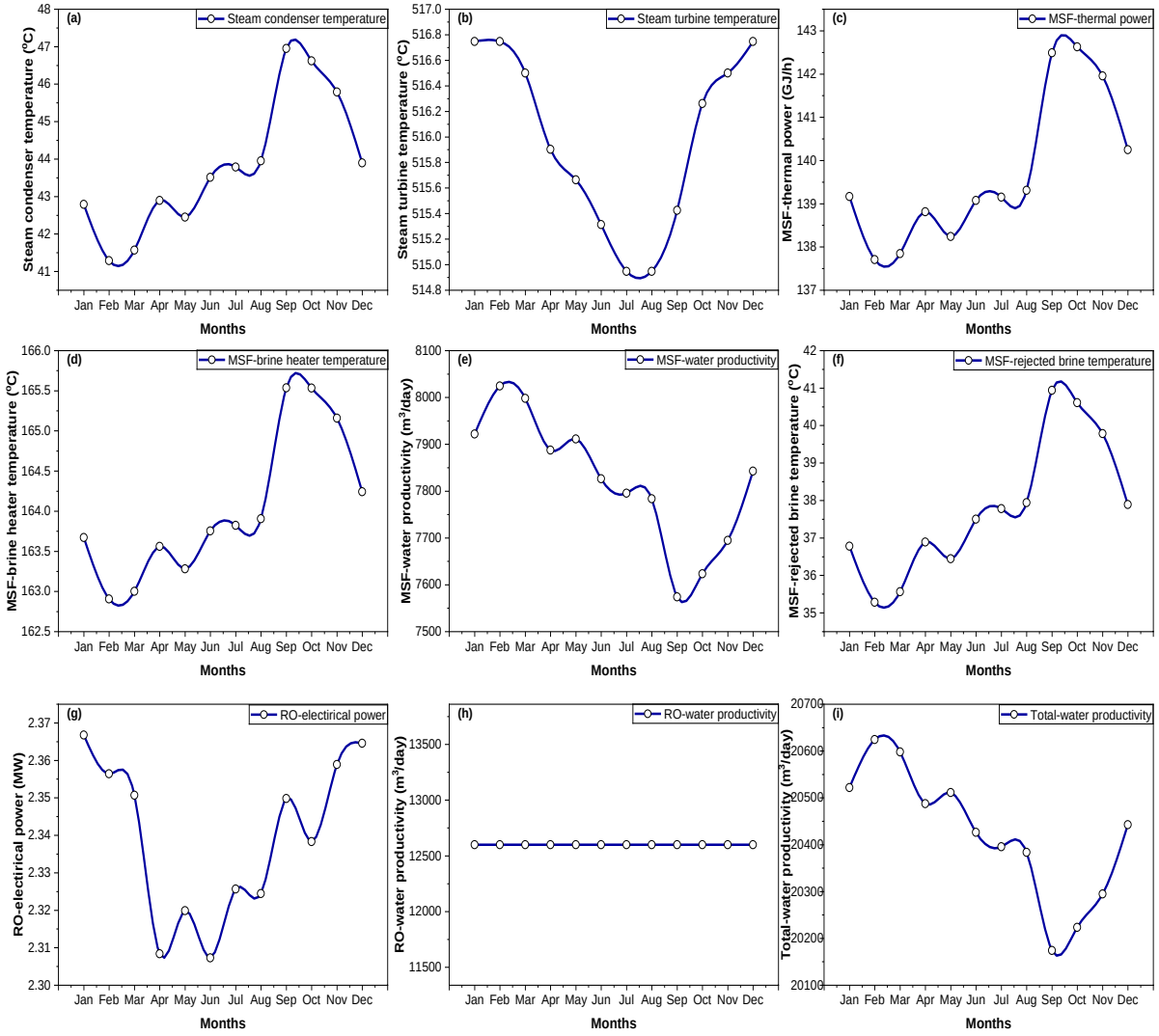

Figure 4. Monthly varaitions in the performance parameters of the steam cycle and MSF-RO unit. (a) steam condenser temperature. (b) steam turbine temperature. (c) MSF-thermal power. (d) MSF-brine heater temperature. (e) MSF-water productivity. (f) MSF-rejected brine temperature. (g) RO-electrical power. (h) RO-water productivity. (i) total water productivity.

Ambient air temperature rises steadily during the spring and summer months. July and August being the hottest months of the year. Consistent with research findings[8, 29, 35-37, 71], rising ambient air temperature gradually reduce the net power output of the cycle, the combined cycle efficiency and freshwater production in conventional thermal desalination units run using streams bled from the steam turbines.

The FCC control strategy was successfully implemented in the simulation model and the flowrate of fuel decreases sharply (Fig(a))in response to rising air temperature and density (Fig(b)).While the minimum power output of the gas turbine (Fig(d)) was observed in July, the minimum power output of the steam turbine (Fig(e)) and the combined cycle efficiency and utilization factor appear to be delayed in the month of September.

The negative cumulative effect of relatively high air ambient temperature and high seawater temperature on the power cycle is more pronounced in September. In this month, the saturation pressure of the steam condenser rose in response to the high steam condenser temperature (Fig(a)). The minimum steam turbine power is accompanied by a maximum of the MSF thermal power in September (Fig(c)).The maximum value of the MSF thermal power is the result of the combined effect of the sharp decline of mass flow rate of the exhaust gases on one hand and a sharp rise in the temperature of the exhaust gases (Fig(c)) on the other hand. Nevertheless, the MSF unit produces the minimum amount of freshwater (Fig(e)) because in September the evaporation range is 54°C. Similar to what was observed in February, the evaporation rate has a dominant effect on freshwater production by the MSF unit. Consistent with this finding, the temperature of the rejected brine is highest (40.94°C) in the month of September as shown in (Fig(f)).

Energy balance calculation of the MSF unit vary in response to monthly changes of the temperature profile of the MSF unit. The seawater feed to the RO unit is 42,000 m^3/dayas shown inFigure 3 (a). Variations in seawater flowrate fed to the MSF unit and in the salinity of the rejected brine are presented in Figure 3 (b) and Figure 3 (c), respectively. It is evident that the salinity of the brine rejected from the MSF unit is markedly lower than the salinity of the brine blown down from the RO unit (Figure 3 (d)). The increase of freshwater production using MSF unit that uses the waste heat of the power cycle has an additional merit related to the relatively lower passive impact of hybrid desalination on the aquatic environment.

The variability in seawater salinity plays a vital role in the efficiency of desalination and power generation systems. Elevated salinity adversely affects heat transfer efficiency in condensers, increasing back pressure and turbine exhaust steam temperature, which subsequently lowers both power output and thermal efficiency in steam turbines Attia [72]. Additionally, higher salinity in cooling water exacerbates these impacts, further reducing overall plant performance. In desalination systems, particularly reverse osmosis, increased salinity raises osmotic pressure, demanding greater energy input for effective operation.

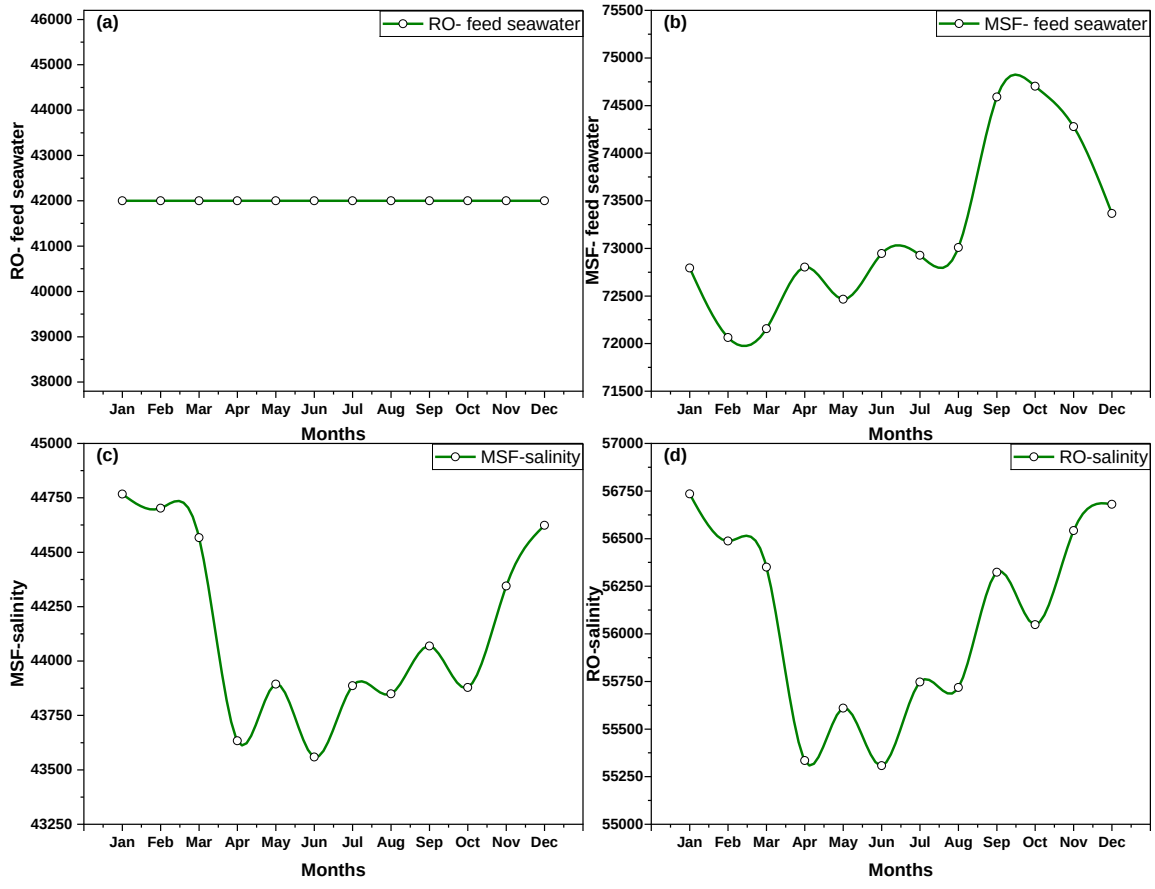

Figure 3. Monthly variations in the operating parameter of the MSF-RO unit. (a) RO-feed seawater. (b) MSF-feed seawater. (c) MSF-salinity. (d) RO- salinity.

3.3. Cost estimation

Table 7presents a detailed breakdown of the system's investment and annual costs at the optimal design point. Additionally, it encompasses the annual maintenance and operational expenses, NOx emission penalties, revenue generation, and payback period for the plant operating under nominal load and ISO conditions.

Figure 4(a) and Figure 4(b) show that the cost of fuel and the penalty cost for producing NOx emissions are influenced by the amount of fuel used, which is in turn affected by air temperature. The highest costs for both the cost of fuel256,818 $/monthand the penalty cost for producing NOx emissions 101,655 $/month are observed in January, February, and December, while the lowest costs 244,795$/monthand 101,578 $/monthare recorded in July and August respectively. These variations are likely due to the impact of air temperature on fuel consumption and emissions.

The net income Figure 4(c) fluctuates throughout the year, with the highest total net income recorded in February 440,833 $/month and the lowest in August 413,246$/month. This pattern correlates with the variations in net power generation and freshwater productivity during the year.

The payback period of the system Figure 4(d) is influenced by fluctuations in maintenance and operation costs. In February, the payback period is at its lowest 4.075 years, indicating higher profitability due to lower costs. On the other hand, August shows the highest payback period 4.558 years, indicating lower profitability due to higher costs. These variations demonstrate how changes in maintenance and operation costs can impact the profitability of the system under different climatic conditions.

Table 7. System investment and operational costs at optimal design point.

Parameter	Nominal load at ISO condition
Air compressor($)	12.564E+06
Combustion chamber ($)	0.0561E+06
High pressure gas turbine ($)	4.6493E+06
Low pressure gas turbine ($)	3.5517E+06
HRSG ($)	4.8970E+06
Steam turbine ($)	12.250E+06
Steam condenser ($)	0.1183E+06
Water pump ($)	0.1713E+06
Seawater pump ($)	0.1039E+06
RO desalination ($)	12.279E+06
MSF desalination ($)	0.5256E+06
Annual investment cost ($/**year**)	9.7961E+06
Annual maintenance and operational cost ($/**year**)	39.071E+06
Annual fuel cost ($/**year**)	38.483E+06
Annual penalty cost for producing NOx emissions ($/**year**)	14.648E+06
Annual total cost (TAC) ($/**year**)	63.515E+06
Annual income received ($/**year**)	68.120E+06
Payback period (**year**)	3.551

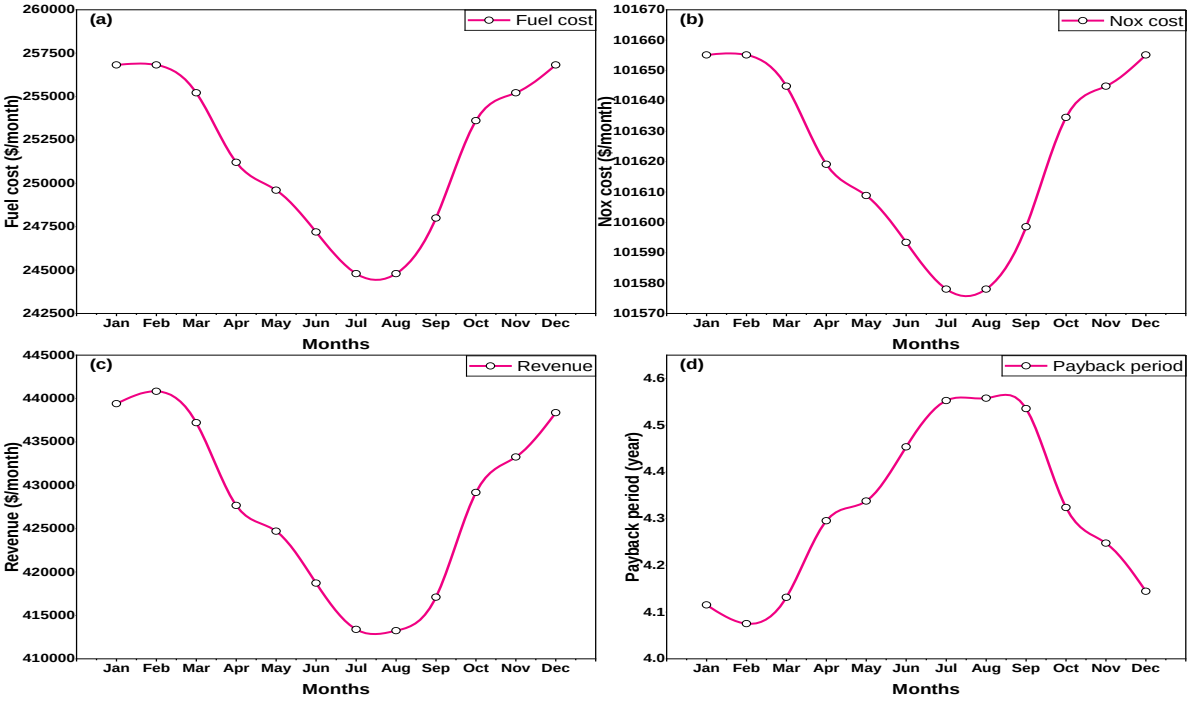

Figure 4. Economic analysis (a) fuel costs. (b) NOx penalties (c) revenue. (d) Payback period under varying ambient conditions.

4. Conclusions

Converting power plants into cogeneration systems is crucial to address the growing demands for energy and freshwater. Conducting comprehensive techno-economic analyses is vital to evaluate the feasibility of transforming combined power plants into dual-purpose systems. The conversion of an existing combined power plant in Port Sudan into a dual-purpose facility for power and freshwater production underscores the critical role of such analyses in project feasibility and optimization.

- A comprehensive once-through multi-stage desalination process was simulated using Aspen HYSYS 10. This model represents the most detailed simulation of its kind to date.
- Freshwater is produced using the waste energy of the power cycle rather than steam streams extracted from the power cycle.
- The study showed that it is possible to power a medium scale MSF desalination unit using the thermal energy of the exhaust gases of the HRSG.
- The simulation model provides a comprehensive assessment of the impact of weather conditions on power and freshwater production.
- Under a monthly fluctuation, the maximum planned net power output reached 177.5MW in February, while the lowest net power output reached 166.3MW in August. Additionally, with a constant water production rate of 12,600 cubic meters per day by the RO desalination unit, the maximum productivity of the MSF unit reached 8,025 cubic meters per day in February, while the lowest productivity reached 7,574 cubic meters per day in September.
- MSF productivity fluctuates within 5% due to monthly weather conditions and was influenced primarily by evaporation range, which is controlled by the seawater temperature.
- Changes in the evaporation range due to seawater temperature variations significantly impact water production from an MSF desalination unit, outweighing the effects of changes in brine heater thermal power.
- The economic analysis reveals that July and August have the lowest costs for both fuel and NOx emission penalties, totaling 346,373 $/month, while January, February, and December incur the highest costs at 358,473 $/month. This information is essential for optimizing the integrated system's operation to minimize expenses and maximize efficiency throughout the year.
- The payback duration of 3.551years is a significant metric, indicating a relatively quick return on investment for the integrated system under ISO conditions. However, the variability in weather conditions and its impact on electricity generation, freshwater productivity, and operating expenses highlight the need for robust strategies to manage these fluctuations effectively. Considering these factors in the system's design and operation can help optimize performance and ensure profitability over the long term.
- The model can be used to assess possible improvements of the design or performance of cogeneration plants. Relevant improvements could include inlet air cooling and control strategies or operating modes of the MSF unit to minimize the effect of weather conditions on the evaporation range.
- The non-uniform salinity of seawater plays a critical role in the performance of desalination and power generation systems. While this research faces challenges in isolating the precise impact of salinity on power output and thermal efficiency, primarily due to the focus on controlling condenser conditions through feed seawater temperature adjustments, it is evident that salinity variations significantly influence desalination systems. Specifically, for RO systems, increased salinity raises osmotic pressure, requiring more power for effective desalination. This underscores the importance of incorporating salinity variations into the design and operation of both CCPP and MSF-RO systems to enhance overall efficiency and reliability.

Acknowledgments

The authors would like to express gratitude to Alexandria University for facilitating this research and providing the necessary resources and facilities for its completion.

References

[1] M. S. Obeidat, E. a. M. Al Abed Alhalim, and B. R. Melhim, "Systematic Approach for Selecting a Cleaning Method to Solar Panels Based on the Preference Selection Index Approach," *Jordan Journal of Mechanical and Industrial Engineering*, vol. 17, no. 3, 2023.

[2] S. Nijmeh, B. Hammad, M. Al-Abed, and R. Bani-Khalid, "A Technical and Economic Study of a Photovoltaic-phase Change Material (PV-PCM) System in Jordan," *Jordan Journal of Mechanical and Industrial Engineering*, vol. 14, no. 4, 2020.

[3] D. Christ and M. KaltschmittQ, "Impact of Decentralized PV Systems Installation on Transmission Lines During Peak Load Situations-Case Study Amman, Jordan," *Jordan Journal of Mechanical and Industrial Engineering*, vol. 13, no. 2, 2019.

[4] S. Kiwan, L. Venezia, F. Montagnino, F. Paredes, and R. Damseh, "Techno-economic analysis of a concentrated solar polygeneration plant in Jordan," *Jordan Journal of Mechanical and Industrial Engineering*, vol. 12, no. 1, 2018.

[5] A. Sakhrieh, W. Shreim, H. Fakhruldeen, H. Hasan, and A. Al-Salaymeh, "Combined solar-geothermal power generation using organic Rankine cycle," *Jordan Journal of Mechanical and Industrial Engineering*, vol. 10, no. 1, 2016.

[6] S. Jaber and A. A. Hawa, "Optimal design of PV system in passive residential building in Mediterranean climate," *Jordan Journal of Mechanical and Industrial Engineering*, vol. 10, no. 1, 2016.

[7] O. Badran, E. Abdulhadi, and R. Mamlook, "Evaluation of solar electric power technologies in Jordan," *Jordan Journal of Mechanical and Industrial Engineering*, vol. 4, no. 1, 2010.

[8] A. H. Abdulrahim and J. Chung, "Comparative thermodynamic performance study for the design of power and desalting cogeneration technologies in Kuwait," *Energy Conversion and Management*, vol. 185, pp. 654-665, 2019.

[9] C. Hanshik, H. Jeong, K.-W. Jeong, and S.-H. Choi, "Improved productivity of the MSF (multi-stage flashing)

desalination plant by increasing the TBT (top brine temperature)," *Energy*, vol. 107, pp. 683-692, 2016.

[10] H. B. Harandi, M. Rahnama, E. J. Javaran, and A. Asadi, "Performance optimization of a multi stage flash desalination unit with thermal vapor compression using genetic algorithm," *Applied Thermal Engineering*, vol. 123, pp. 1106-1119, 2017.

[11] A. Al Bloushi, A. Giwa, T. Mezher, and S. W. Hasan, "Environmental impact and technoeconomic analysis of hybrid MSF/RO desalination: the case study of Al Taweelah A2 plant," *Sustainable Desalination Handbook*, pp. 55-97, 2018.

[12] E. T. Sayed, A. Olabi, K. Elsaid, M. Al Radi, R. Alqadi, and M. A. Abdelkareem, "Recent progress in renewable energy based-desalination in the Middle East and North Africa MENA region," *Journal of Advanced Research*, vol. 48, pp. 125-156, 2023.

[13] A. J. Majeed, G. J. Mohammed, and A. Abdulrazaq, "Sustainable Energy for Water Desalination System Relative to Basra Climate," *Jordan Journal of Mechanical and Industrial Engineering*, vol. 9, no. 2, 2015.

[14] G. M. Tashtoush and M. A. Alzoubi, "An analysis of the Performance and Economic Feasibility of a Hybrid Solar Cooling System that Combines an Ejector with Vapor Compression Cycles, Powered by a Photovoltaic Thermal (PV/T) Unit," *Jordan Journal of Mechanical and Industrial Engineering*, vol. 17, no. 1, 2023.

[15] H. Al Tahaineh and W. Hassan, "Simulation-Design and Performance Analysis of a Small-Scale Concentrating Solar Parabolic Dish System for Hot Water Generation," *Jordan Journal of Mechanical and Industrial Engineering*, vol. 17, no. 3, 2023.

[16] A. Berkane, M. Aksas, and Z. Aouachria, "Performance Study of a Hybrid Solar-Assisted Ground-Source Heat Pump System Used for Building Heating and Hot Water Demands," *Jordan Journal of Mechanical and Industrial Engineering*, vol. 17, no. 4, 2023.

[17] Y. M. Al-Smadi *et al.*, "Assessment and Perception of Renewable Energy Awareness and Potential in Jordan," *Jordan Journal of Mechanical and Industrial Engineering*, vol. 16, no. 4, 2022.

[18] K. M. Bataineh and A. Gharaibeh, "Optimization Analyses of Parabolic Trough (CSP) Plants for the Desert Regions of the Middle East and North Africa (MENA)," *Jordan Journal of Mechanical and Industrial Engineering*, vol. 12, no. 1, 2018.

[19] B. K. Hammad, S. M. Rababeh, M. A. Al-Abed, and A. M. Al-Ghandoor, "Performance Study of On-Grid Thin-Film Photovoltaic Solar Station as a Pilot Project for Architectural Use," *Jordan Journal of Mechanical and Industrial Engineering*, vol. 7, no. 1, 2013.

[20] S. Shalaby, M. E. Zayed, F. A. Hammad, A. S. Menesy, and A. R. Abd Elbar, "Recent advances in membrane distillation hybrids for energy-efficient process configurations: Technology categorization, operational parameters identification, and energy recovery strategies," *Process Safety and Environmental Protection*, 2024.

[21] M. Darwish, H. Abdulrahim, A. Mabrouk, and A. Hassan, "Cogeneration power-desalting plants using gas turbine combined cycle," *Desalination updates*, 2015.

[22] M. Khoshgoftar Manesh, S. Kabiri, M. Yazdi, and F. Petrakopoulou, "Thermodynamic evaluation of a combined-cycle power plant with MSF and MED desalination," *Journal of Water Reuse and Desalination*, vol. 10, no. 2, pp. 146-157, 2020.

[23] A. N. Mabrouk and H. E. Fath, "Technoeconomic study of a novel integrated thermal MSF–MED desalination technology," *Desalination*, vol. 371, pp. 115-125, 2015.

[24] A. M. Pietrasanta, S. F. Mussati, P. A. Aguirre, T. Morosuk, and M. C. Mussati, "Optimization of Cogeneration Power-Desalination Plants," *Energies*, vol. 15, no. 22, p. 8374, 2022.

[25] R. Segurado, L. Alves, N. Duić, and G. Krajačić, "Integrated energy and water planning on an arid island, case of S. Vicente, Cape Verde," *EDITORIAL BOARD*, vol. 4, no. 1, p. 1, 2010.

[26] P. Ahmadi, S. Khanmohammadi, F. Musharavati, and M. Afrand, "Development, evaluation, and multi-objective optimization of a multi-effect desalination unit integrated with a gas turbine plant," *Applied Thermal Engineering*, vol. 176, p. 115414, 2020.

[27] J. I. Manassaldi, M. C. Mussati, N. J. Scenna, T. Morosuk, and S. F. Mussati, "Process optimization and revamping of combined-cycle heat and power plants integrated with thermal desalination processes," *Energy*, vol. 233, p. 121131, 2021.

[28] O. A. Hamed, "Thermoeconomic analysis of combined power cycle integrated with MSF/SWRO desalination plant," *Desalination and Water Treatment*, vol. 57, no. 55, pp. 26552-26561, 2016.

[29] S. Ihm, O. Y. Al-Najdi, O. A. Hamed, G. Jun, and H. Chung, "Energy cost comparison between MSF, MED and SWRO: Case studies for dual purpose plants," *Desalination*, vol. 397, pp. 116-125, 2016.

[30] T. Rensonnet, J. Uche, and L. Serra, "Simulation and thermoeconomic analysis of different configurations of gas turbine (GT)-based dual-purpose power and desalination plants (DPPDP) and hybrid plants (HP)," *Energy*, vol. 32, no. 6, pp. 1012-1023, 2007.

[31] N. M. Wade, "Energy and cost allocation in dual-purpose power and desalination plants," *Desalination*, vol. 123, no. 2-3, pp. 115-125, 1999.

[32] A. Alhawsawi, M. E. Zayed, E. Moustafa, E. Banoqitah, and A. H. Elsheikh, "Hybridizing solar dish Stirling power system with single-effect desalination for sustainable electricity and freshwater co-generation: Mathematical modeling and performance evaluation," *Case Studies in Thermal Engineering*, vol. 45, p. 102997, 2023.

[33] M. M. Aboelmaaref *et al.*, "Design and dynamic numerical modeling of a hybrid reverse osmosis/adsorption-based distillation system driven by solar dish Stirling engine for enhanced performance and waste heat recovery," *Process Safety and Environmental Protection*, vol. 180, pp. 324-338, 2023.

[34] M. E. Zayed *et al.*, "Enhanced performance of a hybrid adsorption desalination system integrated with solar PV/T collectors: Experimental investigation and machine learning modeling coupled with manta ray foraging algorithm," *Applied Thermal Engineering*, vol. 255, p. 124023, 2024.

[35] M. Amiralipour and R. Kouhikamali, "Guilan combined power plant in Iran: As case study for feasibility investigation of converting the combined power plant into water and power unit," *Energy*, vol. 201, p. 117656, 2020.

[36] A. Almutairi, P. Pilidis, N. Al-Mutawa, and M. Al-Weshahi, "Energetic and exergetic analysis of cogeneration power combined cycle and ME-TVC-MED water desalination plant: Part-1 operation and performance," *Applied Thermal Engineering*, vol. 103, pp. 77-91, 2016.

[37] S. Sanaye and S. Asgari, "Four E analysis and multi-objective optimization of combined cycle power plants integrated with Multi-stage Flash (MSF) desalination unit," *Desalination*, vol. 320, pp. 105-117, 2013.

[38] M. Al-Qudah, A. Sakhrieh, A. Almarzouq, and A. Al-Omari, "Thermal Analysis of a Combined Cycle Power Plant under Varying Operating Conditions," *Jordan Journal of Mechanical and Industrial Engineering*, vol. 14, no. 4, 2020.

[39] Q. Jaber, J. Jaber, and M. Khawaldah, "Assessment of power augmentation from gas turbine power plants using different

inlet air cooling systems," *Jordan Journal of Mechanical and Industrial Engineering*, vol. 1, no. 1, pp. 7-15, 2007.

[40] M. W. Shahzad, M. Burhan, and K. C. Ng, "A standard primary energy approach for comparing desalination processes," *NPJ Clean Water*, vol. 2, no. 1, p. 1, 2019.

[41] D.-C. Sue and C.-C. Chuang, "Engineering design and exergy analyses for combustion gas turbine based power generation system," *Energy*, vol. 29, no. 8, pp. 1183-1205, 2004.

[42] K. Al bkoor Alrawashdeh *et al.*, "Performance of dual multistage flashing-recycled brine and solar power plant, in the framework of the water-energy nexus," *Energy Nexus*, vol. 5, p. 100046, 2022.

[43] A. Al-Othman, M. Tawalbeh, M. E. H. Assad, T. Alkayyali, and A. Eisa, "Novel multi-stage flash (MSF) desalination plant driven by parabolic trough collectors and a solar pond: A simulation study in UAE," *Desalination*, vol. 443, pp. 237-244, 2018.

[44] N. A. Moharram, S. Bayoumi, A. A. Hanafy, and W. M. El-Maghlany, "Techno-economic analysis of a combined concentrated solar power and water desalination plant," *Energy Conversion and Management*, vol. 228, p. 113629, 2021.

[45] S. Shaaban, "Performance optimization of an integrated solar combined cycle power plant equipped with a brine circulation MSF desalination unit," *Energy Conversion and Management*, vol. 198, p. 111794, 2019.

[46] M. A. S. Eldean and A. Soliman, "A novel study of using oil refinery plants waste gases for thermal desalination and electric power generation: Energy, exergy & cost evaluations," *Applied energy*, vol. 195, pp. 453-477, 2017.

[47] C. Tian, C. Su, C. Yang, X. Wei, P. Pang, and J. Xu, "Exergetic and economic evaluation of a novel integrated system for cogeneration of power and freshwater using waste heat recovery of natural gas combined cycle," *Energy*, vol. 264, p. 126227, 2023.

[48] W. Weather. "Weather in Port Sudan in 2022." https://world-weather.info/forecast/sudan/port_sudan/2022/ (accessed 4/7/2023.

[49] E. B. Ali *et al.*, "Seasonal variations of hydrographic parameters off the Sudanese coast of the Red Sea, 2009–2015," *Regional Studies in Marine Science*, vol. 18, pp. 1-10, 2018.

[50] H. T. El-Dessouky and H. M. Ettouney, *Fundamentals of salt water desalination*. Elsevier, 2002.

[51] M. M. Alhazmy, "Feed water cooler to increase evaporation range in MSF plants," *Energy*, vol. 34, no. 1, pp. 7-13, 2009.

[52] A. S. Bodalal, S. A. Abdul_Mounem, and H. S. Salama, "Dynamic modeling and simulation of MSF desalination plants," *Jordan Journal of Mechanical and Industrial Engineering*, vol. 4, no. 3, pp. 394-403, 2010.

[53] N. Lior, "Formulas for calculating the approach to equilibrium in open channel flash evaporators for saline water," *Desalination*, vol. 60, no. 3, pp. 223-249, 1986.

[54] A. Soliman, A. G. Alharbi, and M. A. Sharaf Eldean, "Techno-Economic Optimization of a Solar–Wind Hybrid System to Power a Large-Scale Reverse Osmosis Desalination Plant," *Sustainability*, vol. 13, no. 20, p. 11508, 2021.

[55] A. Soliman, A. Al-Falahi, S. Mohamed AEldean, and M. Elmnifi, "A new system design of using solar dish-hydro combined with reverse osmosis for sewage water treatment: case study Al-Marj, Libya," *Desalination Water Treat*, vol. 193, pp. 189-211, 2020.

[56] D.-T. Bălănescu and V.-M. Homutescu, "Performance analysis of a gas turbine combined cycle power plant with waste heat recovery in Organic Rankine Cycle," *Procedia Manufacturing*, vol. 32, pp. 520-528, 2019.

[57] Z. Liu and I. Karimi, "Simulation and optimization of a combined cycle gas turbine power plant for part-load operation," *Chemical Engineering Research and Design*, vol. 131, pp. 29-40, 2018.

[58] M. Shakouri, H. Ghadamian, and R. Sheikholeslami, "Optimal model for multi effect desalination system integrated with gas turbine," *Desalination*, vol. 260, no. 1-3, pp. 254-263, 2010.

[59] F. Alasfour and A. B. Amer, "The feasibility of integrating ME-TVC+ MEE with azzour south power plant: economic evaluation," *Desalination*, vol. 197, no. 1-3, pp. 33-49, 2006.

[60] P. Roosen, S. Uhlenbruck, and K. Lucas, "Pareto optimization of a combined cycle power system as a decision support tool for trading off investment vs. operating costs," *International Journal of Thermal Sciences*, vol. 42, no. 6, pp. 553-560, 2003.

[61] M. H. Khoshgoftar Manesh, R. S. Ghadikolaei, H. V. Modabber, and V. C. Onishi, "Integration of a combined cycle power plant with MED-RO desalination based on conventional and advanced exergy, exergoeconomic, and exergoenvironmental analyses," *Processes*, vol. 9, no. 1, p. 59, 2020.

[62] H. Ghaebi, M. Saidi, and P. Ahmadi, "Exergoeconomic optimization of a trigeneration system for heating, cooling and power production purpose based on TRR method and using evolutionary algorithm," *Applied thermal engineering*, vol. 36, pp. 113-125, 2012.

[63] E. J. C. Cavalcanti, "Exergoeconomic and exergoenvironmental analyses of an integrated solar combined cycle system," *Renewable and Sustainable Energy Reviews*, vol. 67, pp. 507-519, 2017.

[64] C. Park *et al.*, "Stochastic cost estimation approach for full-scale reverse osmosis desalination plants," *Journal of Membrane Science*, vol. 364, no. 1-2, pp. 52-64, 2010.

[65] Y. M. El-Sayed, *The thermoeconomics of energy conversions*. Elsevier, 2013.

[66] M. Rahman, T. K. Ibrahim, and A. N. Abdalla, "Thermodynamic performance analysis of gas-turbine power-plant," *International journal of the physical sciences*, vol. 6, no. 14, pp. 3539-3550, 2011.

[67] C. Deng *et al.*, "Air cooling techniques and corresponding impacts on combined cycle power plant (CCPP) performance: A review," *International Journal of Refrigeration*, vol. 120, pp. 161-177, 2020.

[68] F. J. Millero, R. Feistel, D. G. Wright, and T. J. McDougall, "The composition of Standard Seawater and the definition of the Reference-Composition Salinity Scale," *Deep Sea Research Part I: Oceanographic Research Papers*, vol. 55, no. 1, pp. 50-72, 2008/01/01/ 2008, doi: https://doi.org/10.1016/j.dsr.2007.10.001.

[69] H. B. Harandi, A. Asadi, M. Rahnama, Z.-G. Shen, and P.-C. Sui, "Modeling and multi-objective optimization of integrated MED–TVC desalination system and gas power plant for waste heat harvesting," *Computers & Chemical Engineering*, vol. 149, p. 107294, 2021.

[70] S. M. Alsadaie and I. M. Mujtaba, "Generic model control (GMC) in multistage flash (MSF) desalination," *Journal of Process Control*, vol. 44, pp. 92-105, 2016.

[71] D. A. P. Fernandez, B. Foliaco, R. V. Padilla, A. Bula, and A. Gonzalez-Quiroga, "High ambient temperature effects on the performance of a gas turbine-based cogeneration system with supplementary fire in a tropical climate," *Case Studies in Thermal Engineering*, vol. 26, p. 101206, 2021.

[72] S. I. Attia, "The influence of condenser cooling water temperature on the thermal efficiency of a nuclear power plant," *Annals of Nuclear Energy*, vol. 80, pp. 371-378, 2015.

Supplementary material

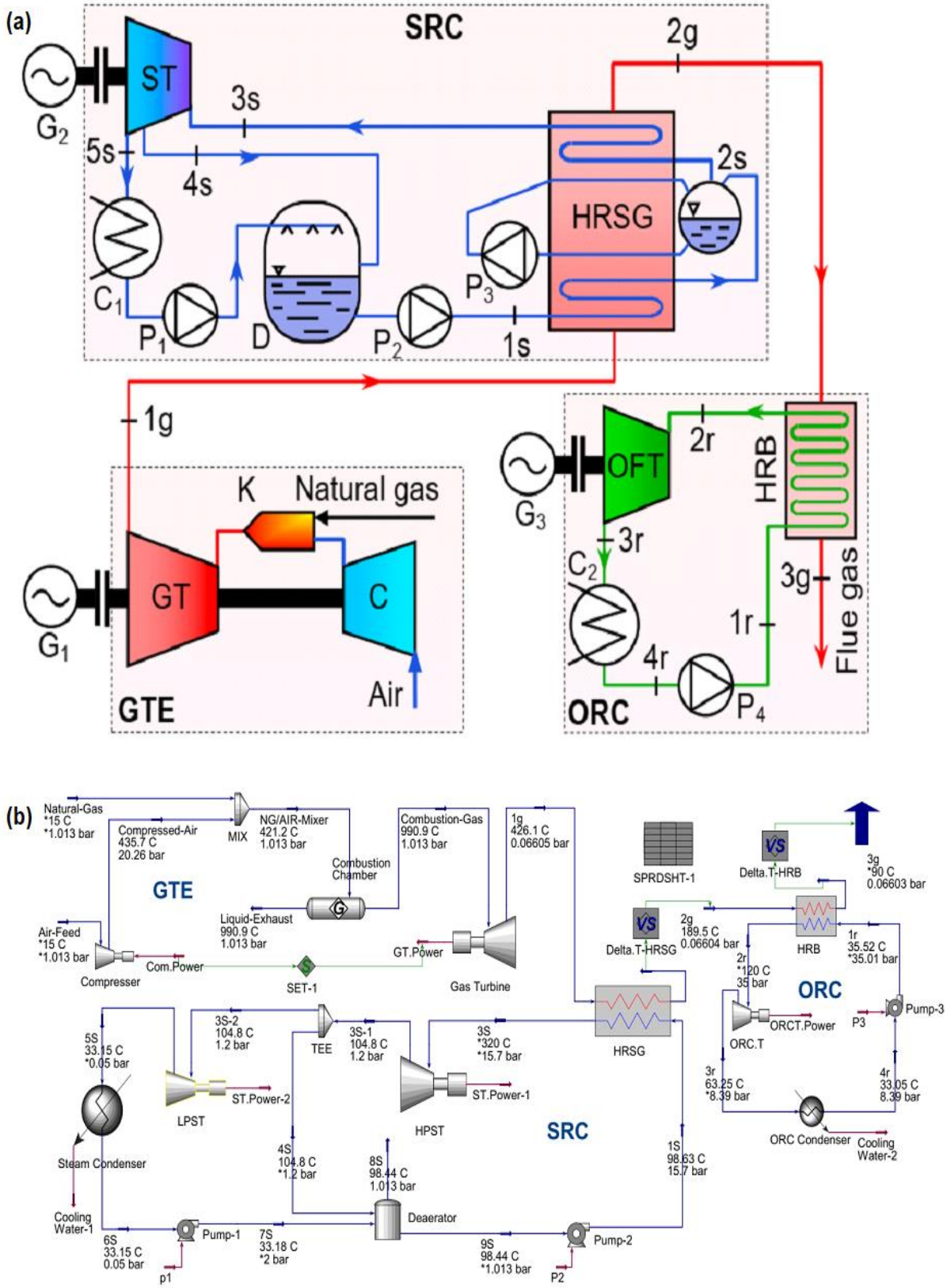

Figure SM 1. Layout of the gas-steam-organic combined cycle (GSO CC). (a) Bălănescu and Homutescu [56] results. (b) model validation results.

Table SM 1. Verification of thermodynamic simulation results of the gas-steam-organic combined cycle (GSO CC) power plant of the different system components.

Parameter	Symbol	Bălănescu and Homutescu [56] results	Model results	Unit	Error %
Air mass flow	$\dot{m}_a$	70.82	70.09	kg/s	1.031
Exhaust mass flow	$\dot{m}_g$	71.09	71.09	kg/s	0.000
gas turbine exhaust (1g)	t_{1g}	426	426.1	℃	0.023
HRSG outlet flue gas (2g)	t_{2g}	188	189.5	℃	0.797
HRB exhaust flue gas (3g)	t_{3g}	90	87	℃	3.333
Gas cycle output	P_{GTE}	16205	16205	kW	0.000
Gas cycle Efficiency	η_{GTE}	34.1	34.1	%	0.000
Steam mass flow	$\dot{m}_{2s}$	6.19	6.19	kg/s	0.000
Extraction steam mass flow	$\dot{m}_{4s}$	0.698	0.698	kg/s	0.000
HRSG inlet water (1s)	t_{1s}	100	98.63	℃	1.370
HRSG outlet steam (3s)	t_{3s}	320	320	℃	0.000
	p_{3s}	15.7	15.7	bar	0.000
Extraction steam (4s)	p_{4s}	1.2	1.2	bar	0.000
Condensation steam (5s)	p_{5s}	0.05	0.05	bar	0.000
Steam cycle output	P_{STE}	4884	4888	kW	0.082
Steam cycle Efficiency	η_{STE}	28.78	28.83	%	0.173
HRB inlet organic fluid (1r)	t_{1r}	--	35.52	℃	--
	p_{1r}	--	35.01	bar	--
Organic mass flow	$\dot{m}_{ORC}$	28.75	28.75	kg/s	0.000
ORC turbine inlet (2r)	t_{2r}	120	120	℃	0.000
	p_{2r}	35	35	bar	0.000
ORC turbine exhaust (3r)	t_{3r}	64	63.25	℃	1.171
	p_{3r}	--	8.39	bar	--
ORC condenser outlet (4r)	t_{4r}	33	33	℃	0.000
	p_{4r}	8.39	8.39	bar	0.000
Organic cycle output	P_{ORC}	741	741.1	kW	0.013
Organic cycle Efficiency	η_{ORC}	10.98	10.97	%	0.091
Overall of GSOCC cycle power	P_{GSOCC}	21830	21834.1	kW	0.018
Overall efficiency of GSOCC	η_{GSOCC}	45.47	45.58	%	0.242

Table SM 2. Performance characteristics of MSF-OT by El-Dessouky and Ettouney [50].

Parameter	Symbol	Value			Unit
Input Parameter					
Feed seawater temperature	T_f	25			℃
Steam temperature	T_s	116			℃
Top brine temperature	T_B	106			℃
Brine temperature in the last stage	T_n	40			℃
Heat capacity of liquid streams	C_p	4.18			℃
Salinity of feed seawater	X_f	42000			PPM
Vapor velocity in the last stage	$V_{v_{24}}$	6			m/s
Brine mass flow rate per stage width	V_b	180			kg/m.s
Weir friction coefficient	C_d	0.5			--
Output Parameter		**Model results**	**El-Dessouky and Ettouney[50] results**	**Error %**	
The distillate flow rate	$\dot{m}_d$	378.8	378.8	0.00	kg/s
The steam flow rate	$\dot{m}_s$	95.49	95.49	0.00	kg/s
The feed flow rate	$\dot{m}_f$	3236.80	3384.8	4.572	kg/s
Performance ratio	PR	3.96	3.96	0.00	--

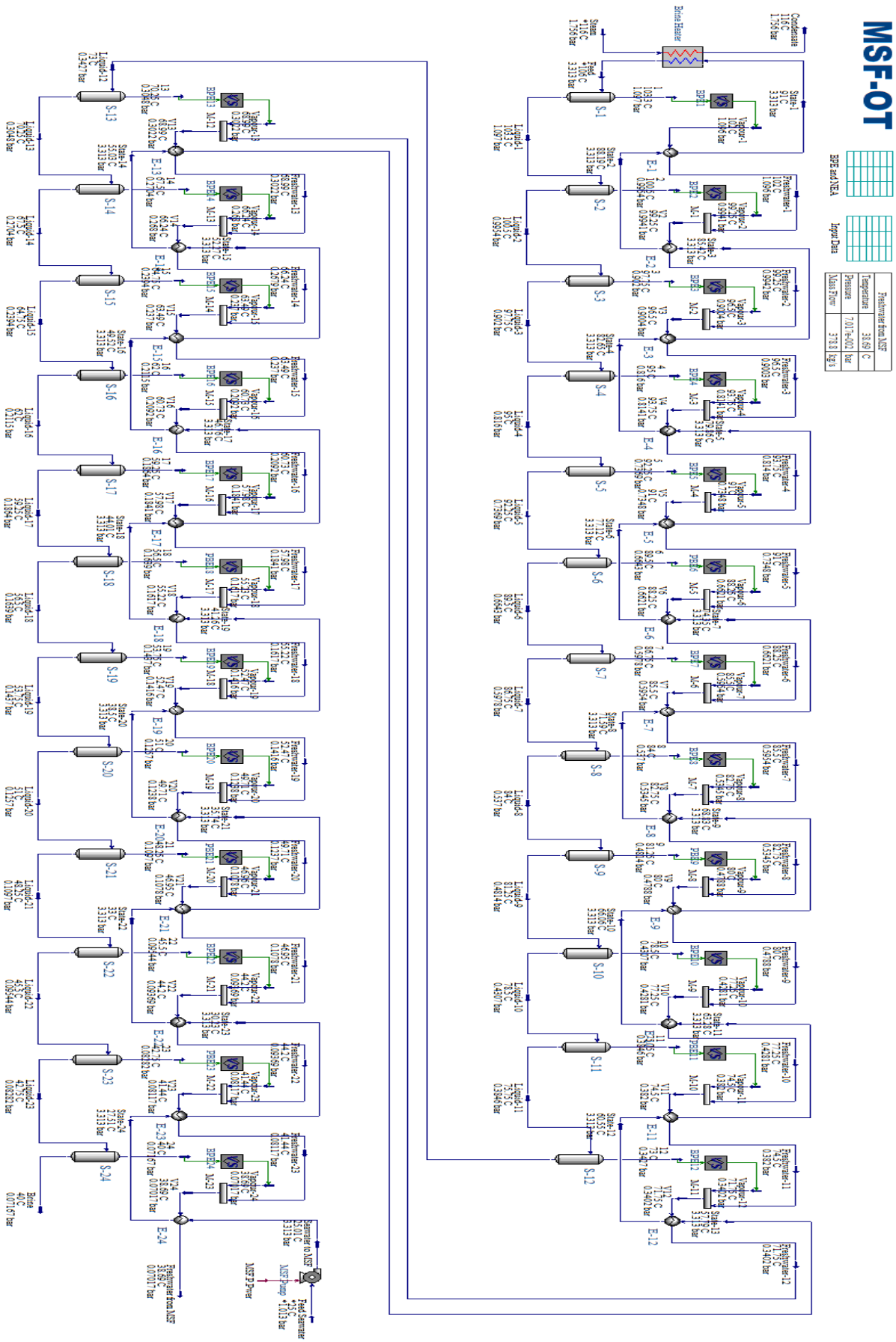

Figure SM 2. Flow diagram of MSF-OT desalination process model validation results.

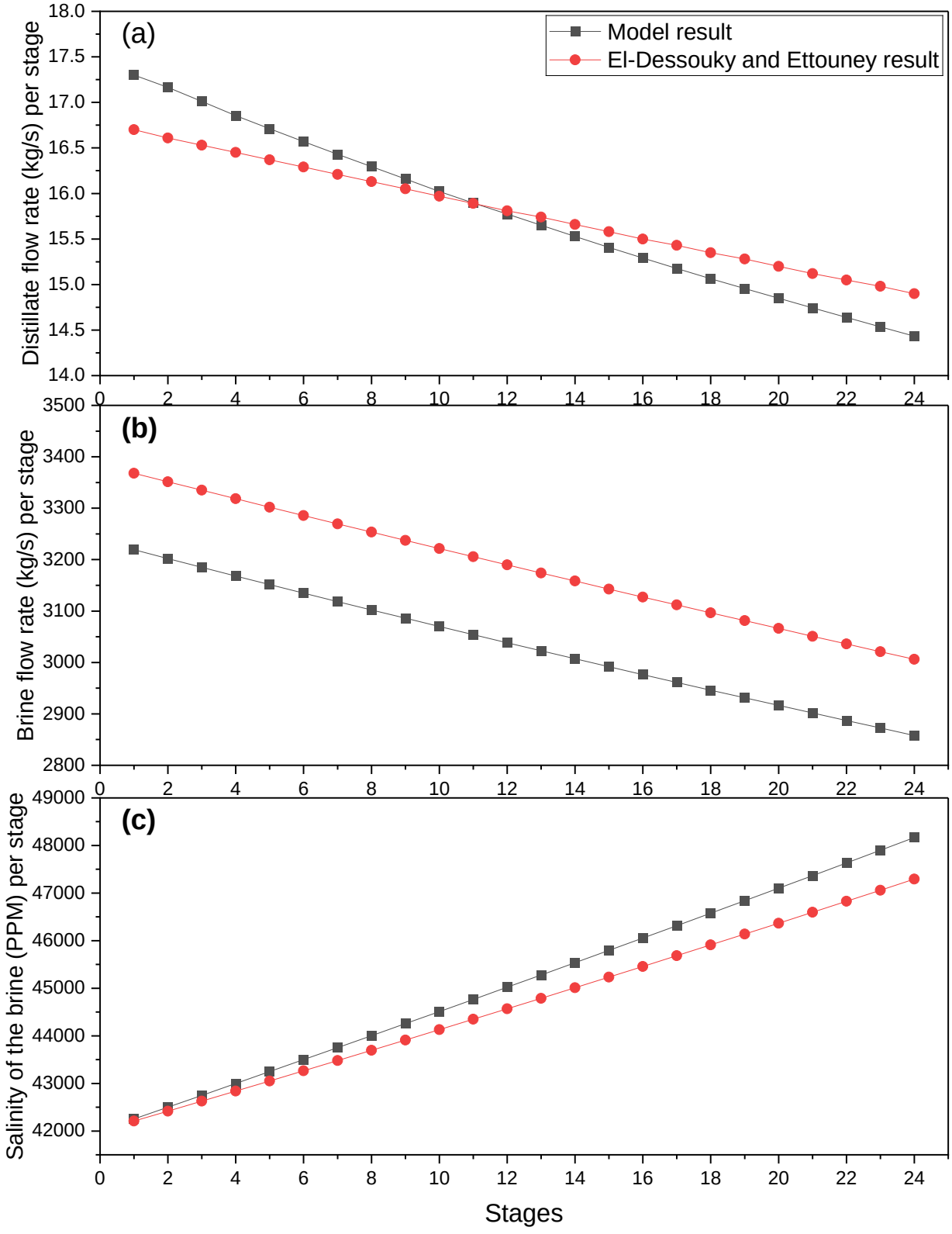

Figure SM 3. Verification of thermodynamic simulation results of the MSF-OT. (a) distillate flow rate. (b) brine flow rate. (c) the salinity of the brine.

Table SM 3. Verification of the temperature simulation results MSF-OT.

Stage	Condensing vapour temperature (oC)			Brine temperature (oC)			Feed seawater temperature (oC)		
	Model result	El-Dessouky and Ettouney [50] results	Error %	Model results	El-Dessouky and Ettouney [50] results	Error %	Model results	El-Dessouky and Ettouney [50] results	Error %
1	101.999	102.002	-0.003	103.250	103.250	0.000	91.000	91.000	0.000
2	99.250	99.254	-0.005	100.500	100.500	0.000	88.186	88.250	-0.073
3	96.500	96.507	-0.006	97.750	97.750	0.000	85.416	85.500	-0.098
4	93.751	93.759	-0.008	95.000	95.000	0.000	82.648	82.750	-0.123
5	91.001	91.011	-0.011	92.250	92.250	0.000	79.862	80.000	-0.173
6	88.251	88.262	-0.012	89.500	89.500	0.000	77.116	77.250	-0.173
7	85.501	85.514	-0.015	86.750	86.750	0.000	74.352	74.500	-0.199
8	82.750	82.765	-0.018	84.000	84.000	0.000	71.588	71.750	-0.225
9	79.999	80.016	-0.021	81.250	81.250	0.000	68.826	69.000	-0.253
10	77.249	77.267	-0.023	78.500	78.500	0.000	66.064	66.250	-0.281
11	74.497	74.518	-0.027	75.750	75.750	0.000	63.284	63.500	-0.341
12	71.746	71.768	-0.031	73.000	73.000	0.000	60.545	60.750	-0.337
13	68.994	69.018	-0.036	70.250	70.250	0.000	57.787	58.000	-0.368
14	66.241	66.268	-0.040	67.500	67.500	0.000	55.029	55.250	-0.400
15	63.488	63.517	-0.045	64.750	64.750	0.000	52.272	52.500	-0.434
16	60.735	60.766	-0.051	62.000	62.000	0.000	49.517	49.750	-0.468
17	57.981	58.014	-0.058	59.250	59.250	0.000	46.763	47.000	-0.505
18	55.226	55.262	-0.066	56.500	56.500	0.000	44.009	44.250	-0.544
19	52.470	52.510	-0.075	53.750	53.750	0.000	41.257	41.500	-0.586
20	49.714	49.756	-0.084	51.000	51.000	0.000	38.505	38.750	-0.633
21	46.956	47.001	-0.096	48.250	48.250	0.000	35.737	36.000	-0.731
22	44.197	44.245	-0.107	45.500	45.500	0.000	33.004	33.250	-0.739
23	41.437	41.486	-0.118	42.750	42.750	0.000	30.226	30.500	-0.897
24	38.689	38.739	-0.129	40.000	40.000	0.000	27.508	27.760	-0.908